HIGH PERFORMANCE AND BREATHABLE PIEZOELECTRIC MEMBRANES FOR SENSING AND ENERGY HARVESTING

A Thesis

Presented to the Faculty of the Graduate School of Cornell University

in Partial Fulfillment of the Requirements for the Degree of Master of Science

by

Minji Kim

August 2014

© August 2014 Minji Kim

ABSTRACT

Multifunctional electronic textiles (e-textiles) or wearable electronics, capable of detecting changes in environmental conditions, monitoring human body functions, and local computation, have enormous potential in everyday and defense applications. One of the major challenges in realizing this potential is to have conformable and effective fiber-based sensors and energy harvesters. My Master's Thesis project seeks to improve the piezoelectric responses of breathable PVDF-based membrane for sensing and energy harvesting, and incorporate the membranes in smart shoes. Specifically, the project explores how the performance of piezoelectric PVDF-based membrane can be improved by adding organosilicate nanoparticles, controlling fiber orientation and the conditions of the electrospining process, and how to embed the membrane sensors in the shoes and interface it with a computer and/or smart phone to monitor foot pressure and body activities.

BIOGRAPHICAL SKETCH

Minji Kim was born December 27, 1987 in Seoul, Korea. She received the Bachelor of Science in Clothing & Textiles from Yonsei University in February 2012. Fall 2012, she started her Master's in Fiber Science and Apparel Design, Cornell University and this is her Master's thesis.

ACKNOWLEDGMENTS

I would like to thank my committee chair, Professor Jintu Fan, who taught me how to think logically as a researcher. I would also like to thank my committee member, Professor Edwin Kan, for sharing his expertise in engineering. My project would have not been possible without support from Cornell Center for Materials Research (CCMR), and my colleagues and friends. Everything I have done was possible from the love of my family.

TABLE OF CONTENTS

LIST OF FIGURES

LIST OF TABLES

LIST OF EQUATIONS

(1) The Scherrer eqeuation: $D = \frac{K\lambda}{B\cos\theta}$

(2) Porosity of membrane: $Porosity(\%) = [1 - \frac{Density_{membrane}}{Density_{polymer}}] \times 100$

2. Background and Justification

2.1. Multifunctional Electronic Textiles (e-textiles) and Wearable Electronics

Clothing has large contact area with skin and it is the most intimate material to human. This unique characteristic makes it highly attractive for sensing human body physiological conditions and energy harvesting. In recent years, considerable attentions and efforts have been directed to the development of multifunctional electronic textiles (e-textiles) or wearable electronics to meet the ever-increasing demands in civil and defense applications. These e-textiles are required to be not only wearable, but also capable of detecting changes in environmental conditions, monitoring human body functions, local computation as well as wireless communication [1-3].

A team in Georgia Tech [4] pioneered the integration of a flexible data bus into the T-shirt structure for transmitting the information to monitoring devices such as an Electrocardiography (ECG) machine, a temperature recorder, a voice recorder, etc. This smart T-shirt was considered to have potential applications in areas ranging from combat to geriatric care. Sensory baby vest for monitoring infants have also been developed by Linti et al. [5], which is easier to handle and less obtrusive than the commonly used medical systems. ECG and respiratory frequency sensors have been integrated into swim suits to provide information to trainers during training [6]. Sensorized garments measuring ECG, temperature, breathing and SpO_2 [7] and a glove capable of monitoring skin temperature (SKT), photoplethysmography (PPG), and galvanic skin response (GSR) [8] have been developed and their performances were evaluated. Smart shoes have also been instrumented with piezoelectric sensors for sensing pressure and harnessing mechanical energies [9-11].

Key user requirements of smart clothing are functionality, performance metrics, durability, maintainability, usability in field, and wearability. Requirements for good wearability are comfortable, no skin irritation, lightweight, breathable (air permeable), moisture absorption, easy to wear and take off, easy to access body, and maintain range of motion [12]. The challenge in developing multifunctional smart clothing is to achieve intelligent functionality without undue sacrifice in durability, maintainability and wearability. Very often, the excessive weight and cumbersome, the lack of sufficient mobile power supply, and poor maintainability and wear comfort prohibit such smart clothing from wide adoption by consumers.

2.2. Piezoelectric Materials

Piezoelectric material is the one that undergoes a change in electrical polarization in response to mechanical stress or vice versa [10, 13]. This property makes piezoelectric material a potential material for sensors, transducers, actuators and energy harvesters. Generally speaking, piezoelectric materials can be divided into two main groups: ceramics and polymers. Piezoelectric ceramics [e.g. Lead zirconate titanate (PZT)] and piezoelectric polymers [e.g. PVDF and its co-polymers] have been used in wearable electronics [14-19]. Although piezoelectric ceramics have been used successfully in many applications, they have some significant drawbacks: limited deformation, brittleness, high mass density and toxicity when containing lead. Piezoelectric polymers are considered to be favorable for wearable electronic applications due to its thin, flexible, and deformable characteristics [20]. However, lack of breathability and relatively lower piezoelectricity limit the applications of piezoelectric polymer films. This limitation can be alleviated when piezoelectric polymers are electrospun into membranes. Breathable, lightweight, soft and flexible piezoelectric membranes are desirable in

many applications apart from smart clothing, such as, biomedical materials, polymer electrolytes and filtration membranes [21-23].

Polyvinylidene fluoride (PVDF) and poly(vinylidene-trifluoroethylene) [P(VDF-TrFE)] are the most frequently used piezoelectric polymers due to its strong ferroelectric, piezoelectric, and pyroelectric properties [24-25]. Piezoelectric properties of piezoelectric membranes can be characterized by measuring d_{33} values or crystallinity [26]. Among piezoelectric polymers, PVDF and its' copolymer's piezoelectricity can be investigated by crystalline structure, fraction of polar β–phase [27]. The biggest challenges which limit the wider application of electrospun polymeric piezoelectric membrane are relatively weak piezoelectric response and mechanical strength. My project is therefore aimed at investigating the effect of adding organosilicate nanoparticles in P(VDF-TrFE), controlling fiber orientation and the processing parameters of electrospining on the strength and piezoelectric responses. Furthermore, I will explore the application of such membranes as sensors embedded in the sports shoes and the interface with a computer and/or smart phone for monitoring foot pressure and body activities.

This project will improve the understanding of the relationship between properties, structure and processes of porous polymeric piezoelectric materials, and demonstrate the feasibility of using electrospun piezoelectric membranes in smart clothing.

3. Objectives

The specific objectives of the project are:

I. To investigate how the additional organosilicate nanoparticles in P(VDF-TrFE) affect the structure, strength and piezoelectricity of electrospun P(VDF-TrFE) membrane.

II. To investigate the effect of fiber orientation on the structure, strength and piezoelectricity of electrospun P(VDF-TrFE) membrane.

III. To investigate the effect of processing parameters of electrospinning process on the structure, strength and piezoelectricity of electrospun P(VDF-TrFE) membrane.

IV. To develop a prototype smart shoe system incorporating breathable P(VDF-TrFE) membrane for sensing foot pressure and monitoring body activities.

To improve the sensitivity of piezoelectric membranes for application as sensors and energy harvesters, higher coupling coefficient is necessary. A potential solution resides with electro-spinning parameters to gain the best piezoelectricity within the same polymer. Better piezoelectricity is expected by greater extension and better fiber orientation as they can result in better-aligned crystal axes. This can be achieved by increasing the collecting drum rotation speed.

Weak mechanical properties have also limited wide usage of piezoelectric materials. Dr. He first demonstrated that adding organosilicate into P(VDF-TrFE) membranes can significantly improve its mechanical properties without compromising its lightness in weight, breathability, and porosity. However, he did not conduct systematic investigation on how the quantity of organosilicate affect the structure, mechanical property and piezoelectric properties of PVDF/P(VDF-TrFE) membranes. Systematic comparison of composite P(VDF-TrFE)

membranes containing zero, two, four, six, eight and ten percent of organosilicate are carried out in this project. Also compressive pressure to evaluate piezoelectric response was modified from 0.33MPa to 0.07MPa which is in the range of human foot pressure range, 0-0.20MPa, in order to test porous piezoelectric membranes' potential to be used as foot pressure sensors [49].

Foot pressure sensors provide wearers the information of their pressure map and their lifestyle. Foot pressure map will be useful in health and sports area. In health care, foot pressure map can be used orthopedically, helping diagnose the cause of the health problem and find a cure. In terms of life style, foot pressure data can be converted into activity data along with map. Electrospun porous piezoelectric membrane does not compromise comfort for its breathability and therefore a good material for everyday or longtime use sensors.

While pressure sensing has many applications, for example, the monitoring of blood pressure can be used to predict numerous blood pressure related risks [28, 29], the present project is focused on measuring foot pressure. The usefulness of the developed piezoelectric membrane sensor as well as its integration with computer or mobile devices will be demonstrated. This work should provide a foundation of using piezoelectric membrane sensors for various applications.

4. Methodology

The strong electric field in electrospinning creates the piezoelectric phase of PVDF and its copolymers directly from their solution in one step avoiding the time-consuming electric field poling process. The electrospinning process involves the uniaxial stretching of a viscous polymer solution or melt in an electric field due to electrostatic repulsions between surface charges along the jet. When a voltage is applied, the pendant droplet at the syringe tip becomes electrified, and is distorted into a conical shape. This distortion, known as the Taylor cone, is due to the electrostatic repulsion between the surface charges and the Coulombic force exerted by the external electric field [30]. When a sufficiently high voltage is applied, the electrostatic repulsion between surface charges overcomes the surface tension of the solution, and an electrified jet of polymer solution is ejected from the syringe tip. As the jet extends, the solvent evaporates leaving a solid fiber [31, 32].

Electrospun PVDF and its copolymer membranes have numerous advantageous characteristics over films for high porosity, lightweight, excellent pliability and good breathability. However, the poor mechanical property limits its applications since a small fracture can lead to serious consequences in the end-use. For example, Yang et al. have demonstrated that the main deficiency in the fabricating PVDF membrane separators process by electrospinning was low mechanical property, which induced partial short circuits inside the cells [33]. Na et al. attempted to improve the mechanical properties of electrospun PVDF membrane by hot-pressing [34-36]. Nevertheless, hot-pressing compromises membrane’s advantageous characteristics in terms of high porosity, lightweight, good breathability, and piezoelectricity.

The fabrication of durable, porous and highly flexible piezoelectric materials is possible through the usage of fillers. F. He applied organosilicate nanoparticles to P(VDF-TrFE) membranes. Comparison of pure PVDF/P(VDF-TrFE) membranes, and 4% and 10% of P(VDF-TrFE)/organosilicate composite membranes showed significant improvements in strength, modulus, extensibility, and toughness. Using organosilicate as fillers did not compromise high porosity, low density, good breathability and piezoelectricity of the membranes.

Composition of 4% organosilicate had better mechanical property and higher charge output than 10% organosilicate composite membranes. More systematic work is needed to determine whether 4% organosilicate is the best ratio for durable P(VDF-TrFE) membranes. Additional research of 2%, 6% and 8% organosilicate composite P(VDF-TrFE) membranes were conducted to seek the best ratio of organosilicate to improve mechanical property of P(VDF-TrFE) membranes.

Although using organosilicate as fillers did increase mechanical property of P(VDF-TrFE) membranes, it compromises membrane's piezoelectricity. Lower charge output was observed on organosilicate composite membranes compared to pure P(VDF-TrFE) membranes. In terms of piezoelectric membranes, improving coupling coefficient without compromising breathable benefit is important if to be used in clothing. The piezoelectric effect is due to each molecule that makes up the crystal is negatively charged in one end, and positively charged on the other end. This polarization is called a dipole. The polar axis is the line that connects the positive charge and the negative charge. In a monocrystal, all polar axes align in same direction. This makes the crystal symmetrical because any arbitrary cut of the crystal yields two crystals with same polar

axes direction as the original crystal. In a polycrystal, different parts have different polar axes therefore making polycrystal asymmetrical. Two crystals cut from a polycrystal could not yield same polar axes. Figure 1 illustrates this concept.

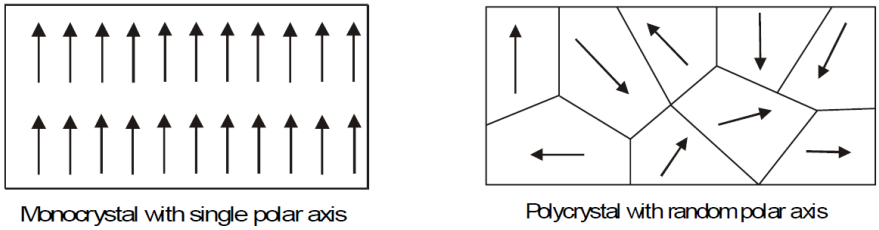

Figure 1. Mono vs. Poly Crystals.

Polycrystal can attain piezoelectric effect by being heated under the application of a strong electric field. The heat allows the molecules to move more freely and the electric field forces all of the dipoles in the crystal to line up and face in nearly the same direction (Figure 2).

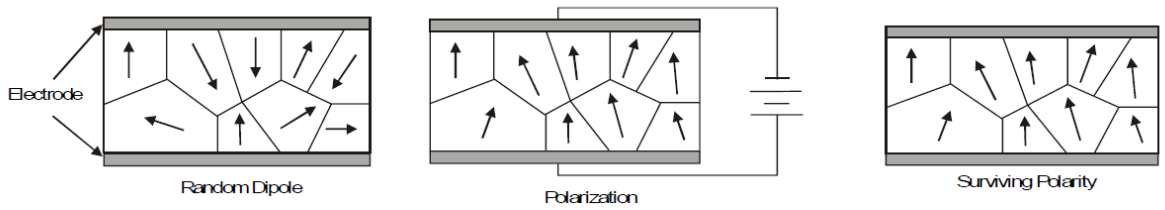

Figure 2. Polarization of Ceramic Material to Generate Piezoelectric Effect.

This process is called poling. Poling is unnecessary with electrospun membranes because molecules are available to move and aligns dipoles under the electric field used to extract fibers [37, 38]. Various studies have been carried out on electrospinning conditions and piezoelectric sensitivity. Kim et al., made sensors based on PVDF fabrics. Inorganic salts were embedded to fabrics to increase their piezoelectric sensitivity. However an additional step of removing the salts was needed before the application [37]. P(VDF-TrFE) is one of the most important PVDF

copolymers as it can form β-phase crystallites automatically at room temperature. F. He et al investigated the fabrication process and properties of electrospun P(VDF-TrFE) copolymers nanofibres and membranes and further hot pressing to prepare piezoelectric nanofibrous membranes [38]. However, hot pressing compromises breathability by blocking some pores. Thus, method with no further treatment before application or compromising breathability is necessary. Different collecting speed can yield membranes with more oriented fibers. More oriented fibers would have same effect as more oriented dipole axes thus, expected to have better electrical property performance than the membranes with randomly oriented fibers. Controlling fiber orientation requires no further treatment or no mechanical alterations of membranes. Better fiber orientation is expected by increasing the collecting drum rotation speed.

PVDF and its copolymers can crystallize in five different forms: α, β, γ, δ and ε. The polarization behavior and ferroelectric properties depend strongly on the processing conditions and resulting crystal structures. Among these structures, the most readily formed crystal structure is the α-form. This form consists of non-polar anti-parallel chains. In contrast, the β-crystalline form is a polar structure. Therefore, samples with higher β-phase fractions are expected to display stronger ferroelectric polarization [39]. Analysis of the crystalline structure can be investigated by Fourier transform infrared (FTIR) spectroscopy and Wide-angle X-ray Scattering (WAXD). FTIR data, the characteristic absorption bands designated for the α phase of PVDF at 490 cm^{-1}, 764 cm^{-1}, 975cm^{-1}, and 1402 cm^{-1}. The absorption bands for the β phase is at 510 cm^{-1}, 600 cm^{-1}, 840 cm^{-1}, and 1276 cm^{-1} [39, 40]. The amorphous halo (2θ ~19˚) in the WAXD pattern indicates amorphous α phase. Two theta (2θ) value about 22˚ is the area that corresponds to the β phase

[41]. Morphology of the electrospun membranes can be observed by scanning electron microscope (SEM) and transmission electron microscopes (TEM). Further analysis is possible with fast Fourier transform (FFT) to analyze the degree of fiber alignment based on the conversion of the image into frequency spacing [42].

5. Materials and Methods

5.1. Materials

5.1.1. Polymer

Poly(vinylidene-trifluoroethylene) was acquired from Measurement Specialties Inc. (Hampton, VA) in powder form. This P(VDF-TrFE) copolymer has 80:20 % in molecular (VDF-TrFE).

5.1.2. Filler

The organically modified clay (DK4 OMMT) was generously given by Fenghong Clay Company in the form of powder.

5.1.3. Other Materials

The commercial PVDF solid film (110 micron in thickness) is kindly supplied by Measurement Specialties in USA.

Conductive thread, polyethylene terephthalate fibers coated with silver, was purchased from Lamé Lifesaver. This thread has a resistance of approximately 0.85ohm /cm.

5.2. Methods

5.2.1. Solution Preparation

Polymer solutions of 16wt% for electrospinning were prepared by dissolving P(VDF-TrFE) powders in DMF-acetone(70 vol% : 30 vol%). Magnetic stirring method on a hot plate was used to melt the polymers into the solvent. To evenly disperse organosilicate powder, sonication method was used.

5.2.1.1. Organosilicate Composite Solution

Different weight percentage of organosilicate was added to the polymer solution to investigate the effect of addition of organosilicate to P(VDF-TrFE) membrane. 2, 4, 6, 8, and 10 wt% of organosilicate composite solution was prepared by the method explained above.

5.2.2. Electrospinning

Piezoelectric P(VDF-TrFE) membranes are prepared by electrospinning. The electrospinning apparatus consisted of a high voltage power supply, a syringe pump, a needle (23 G), and a cylindrical drum collector. Spinning parameters for organosilicate composite membranes are a cylindrical drum collector (outer diameter: 100mm), the solution flow rate of 0.3 ml/h, the spinning distance between the needle tip and the collector was 15 cm, and the applied direct current (DC) voltage 21kV. Membranes with different degree of fiber orientation can be obtained by varying collector rotating speed. Three different collector rotation speed of 140, 2000, 4000 rotation per minute (rpm) was used to fabricate membranes with different degree of fiber orientation. Other spinning parameters for membranes with different fiber orientation are, a cylindrical drum collector (outer diameter: 62mm), the solution flow rate of 0.4 ml/h, the spinning distance between the needle tip and the collector was 10 cm, and the applied direct current (DC) voltage was 14kV.

5.2.3. Piezoelectric Response

The measurement setup of pressure sensors made from piezoelectric membranes is shown in Figure 3. Piezoelectric responses of piezoelectric membrane will be measured by using

customized equipment; Instron 5566 machine in compression mode produces the compressive pressure and a digital electrometer (Fluke 8846A) combined with a lab charge amplifier (Piezo Film Lab Amplifier Measurement Specialties) measures the voltage output. Two metal foils will be attached on both sides of the piezoelectric membrane as electrodes [43].

5.2.3.1. Organosilicate Composite Membrane

Membranes were tested with impact pressure of 3.33 MPa.

5.2.3.2. Different Fiber Orientation Membrane

Impact pressure of 0.07 MPa was selected within human foot pressure range 0-0.20MPa [49].

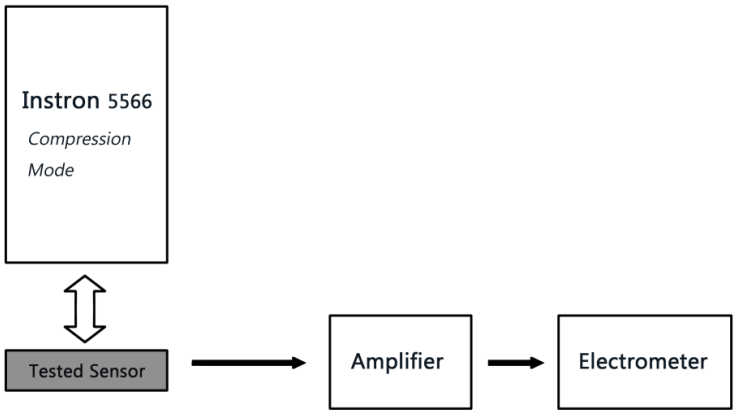

Figure 3. Setup of Piezoelectric Sensors Piezoelectric Response Measurement.

5.2.4. Smart Shoe Prototype

To obtain accurate and reliable pressure map of foot, the embodiment of membrane sensors, circuitry design and interfacing with wireless devices will be carefully considered. The pressure measurement system is envisaged to have a wireless micro-controller, breathable membrane pressure sensors and a mobile phone. The micro-controller is programmed to capture the pressure data from the sensors and communicate with the mobile phone. Figure 4 illustrates the

envisioned system. Piezoelectric membrane sensors generate impedance data when pressure is applied and wireless micro controller converts the analog impedance data to digital and transmits to transponder.

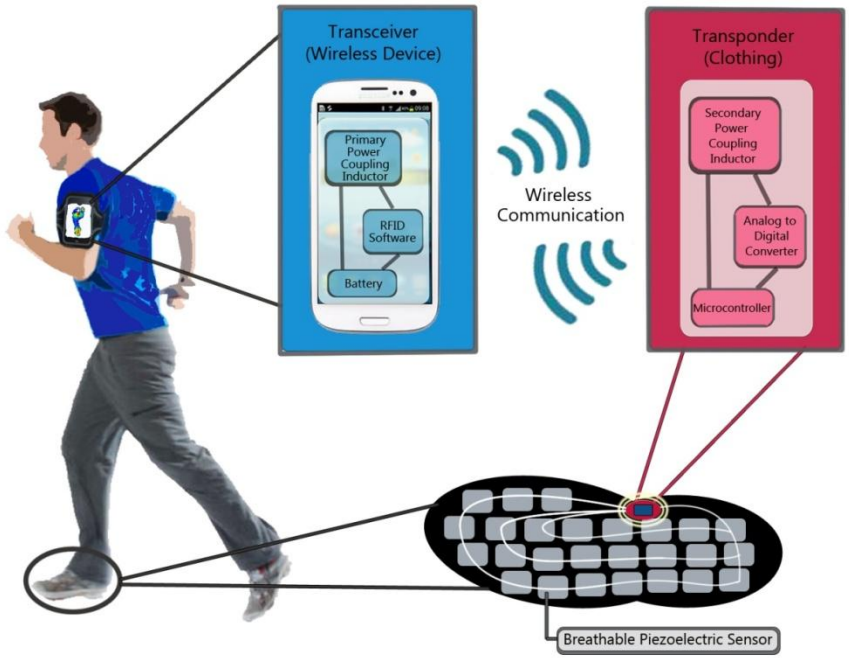

Figure 4. Envisioned system of Breathable Piezoelectric Sensor.

In fabricating the piezoelectric membrane sensors, solution and spinning parameters should be carefully chosen to obtain membranes with desired electrical properties for use as foot pressure sensors. It should be able to detect up to 100% of the human weight, and sensible enough to read 5% of the human weight to distinguish pressure between different foot area.

5.2.5. Fiber and Membrane Characterizations

To characterize the fibers and membranes, scanning electron microscopy (SEM), transmission electron microscopy (TEM), differential scanning calorimetry (DSC), Wide-angle X-ray

Scattering (WAXD), fourier transform infrared spectroscopy (FTIR), tensile test, and the water vapor transmission rates (WVTRs) were used. To obtain images of nanofiber mats, SEM(Carl Zeiss, LEO 150) was utilized. The fiber orientation in membranes, and fiber diameters were analyzed from the SEM images using image analysis software (Image J, National Institutes of Health, USA). TEM(FEI, T12) was used to obtain visual image of organosilicate located in the fibers. To determine the effect of organosilicate and collector rotation speed on crystallinity and crystalline type, DSC, WAXD, and FTIR was used. The DSC measurements were taken using a differential scanning calorimeter (TA instrument, Model No. 2000) at nitrogen atmosphere. Temperature was equilibrated at 25℃ and heated 10 ℃/min to 65℃. Isothermal state at 65℃ was maintained 1 minute and then cooled to 30℃ with rate of 10℃/min to erase thermal history. The sample was reheated to 220℃ with rate of 10℃/min. The Wide-angle X-ray Scattering patterns were taken at room temperature using a Scintag diffractometer (Scintag, Theta-Theta Diffractometer) with Cu as the standard target, $\lambda = 1.5405$Å, and line source 1 x 10 mm. FTIR was carried out with 64 number of scans, and resolution of 4 (Nicolet Magna-IR 560 Spectrometer). Tensile testing was done with sample size of 10mm x 25mm, and strain rate of 5mm/min (Instron 5566). The water vapor transmission rates (WVTRs) was measured with cup test method (BS 7209). Measurement was done in controlled environment where temperature and relative humidity is maintained at 21.1℃ and 65% respectably. The density of electrospun membranes were calculated by dividing measured mass by measured volume.

SEM, TEM, WAXD are located in the Cornell Center for Materials Research (CCMR). DSC, FTIR, and Instron are located in Human Ecology Building, Cornell.

6. Results and Discussion

6.1. Organosilicate Composite Membranes

6.1.1. Piezoelectric Response

Piezoelectric responses of piezoelectric membrane were measured by using customized equipment; Instron 5566 machine in compression mode produces the compressive pressure and a digital electrometer (Fluke 8846A) combined with a lab charge amplifier (Piezo Film Lab Amplifier Measurement Specialties) measured the voltage output.

Electrometer will be controlled by a LabView program to measure the piezoelectric responses of breathable P(VDF-TrFE) membrane. Voltage output will be stored in text file which can be imported to excel. Excel will be used to analyze the voltage output.

Improving mechanical property of P(VDF-TrFE) porous membranes by adding organosilicate was originally done by F. He. Pure P(VDF-TrFE) membrane, 4 wt%, and 10 wt% organosilicate composite P(VDF-TrFE) membranes have been compared by He. He have concluded 4 wt% organosilicate composite have the most mechanical improvements. However, his work did not systematically investigate the effect of changing percentage (0~10 wt%) of organosilicate. Therefore, I have studied effect of organosilicate on P(VDF-TrFE) membrane with pure P(VDF-TrFE), 2 wt%, 4 wt%, 6 wt%, 8 wt%, and 10 wt% organosilicate composite P(VDF-TrFE) membranes.

The compressive piezoelectric responses and maximum voltage output of a non-piezoelectric PET solid film, a commercial piezoelectric PVDF solid film, and electro spun porous membranes

are shown in Figure 5. PET solid film has no voltage output signal which confirms piezoelectricity of the piezoelectric film and membranes. Voltage output signals have two opposite peaks which correspond to piezoelectric response of pressure input and release [43, 48].

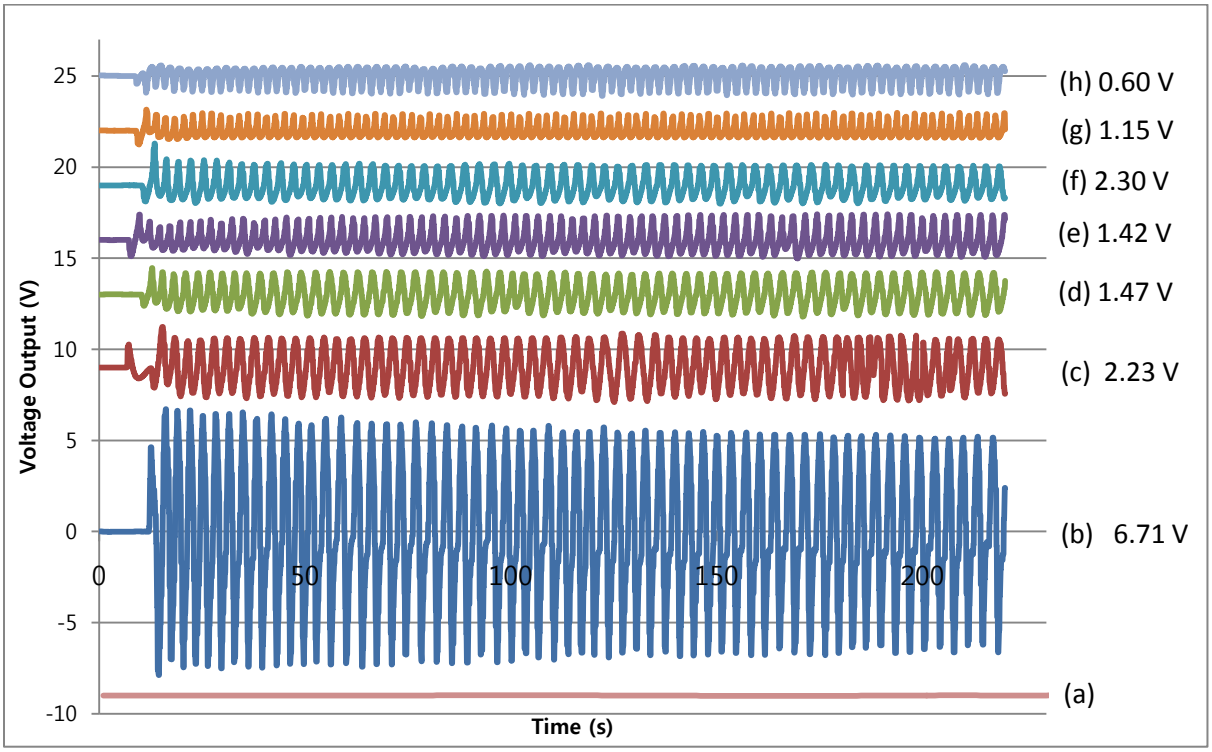

Figure 5. The piezoelectricity curve and peak value of voltage output of (a) non-piezoelectric PET solid film, (b) commercial piezoelectric PVDF solid film, (c) electrospun P(VDF-TrFE) membrane, (d) 2% SiO_2, (e) 4% SiO_2, (f) 6% SiO_2, (g) 8% SiO_2, and (h) 10% SiO_2.

Maximum voltage output data is shown in Figure 6. As more organosilicate is added, voltage output generally decreases except for 6wt% organosilicate P(VDF-TrFE) membrane sample. This could be due to the higher crystallinity or crystal size which will be discussed later with WAXD data.

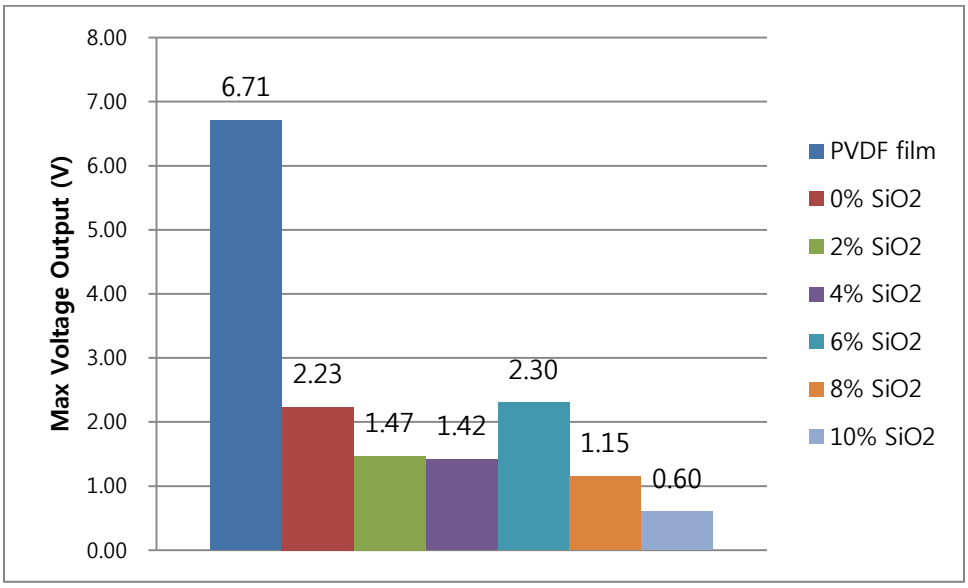

Figure 6. Maximum voltage output of PVDF film, pure and organosilicate composite P(VDF-TrFE) membranes.

6.1.2. Fiber and Membrane Characterizations

6.1.2.1. SEM

Figure 7 shows SEM images of pure (a)P(VDF-TrFE) membrane, and P(VDF-TrFE)/ organosilicate composite membranes with different weight percentage of organosilicates. Very little beading and randomly oriented nanofibers were visually confirmed with SEM images. The fiber diameters of the membrane samples were evaluated by the mean of more than 50 measurements. The averages of fiber diameter measurements are shown on Figure 8. There is a tendency of decrease of fiber diameter as the weight percentage of organosilicate increases. Other studies also found P(VDF-TrFE)/organosilicate composite membranes have finer fibers than pure P(VDF-TrFE) membranes. Enhanced electrical conductivity of the electrospinning solution containing organosilicate is believed to be the cause [45-47].

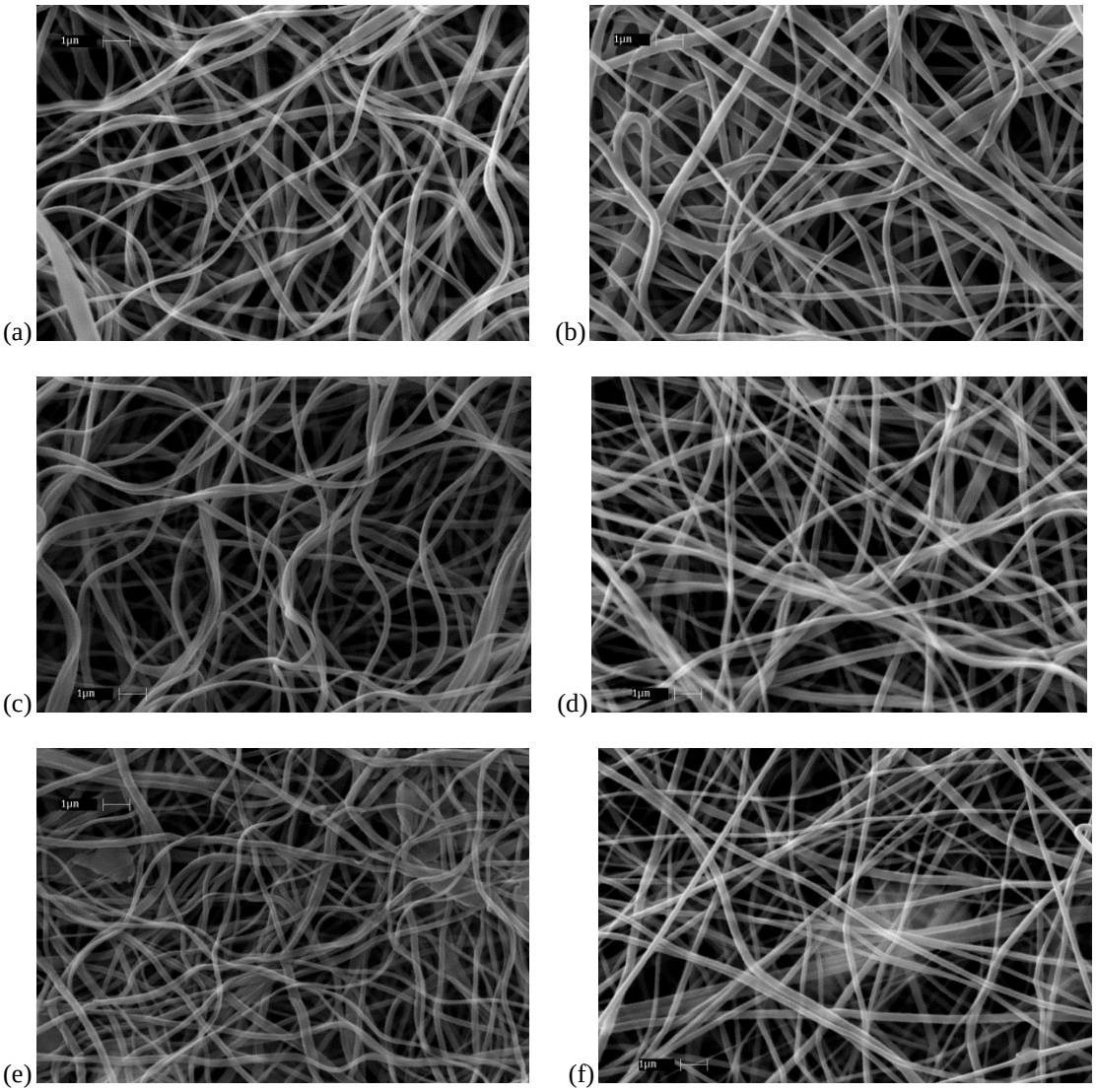

Figure 7. The SEM images of pure (a)P(VDF-TrFE) membrane, (b) 2% SiO_2, (c) 4% SiO_2, (d) 6% SiO_2, (e) 8% SiO_2, and (f) 10% SiO_2 composite membranes.

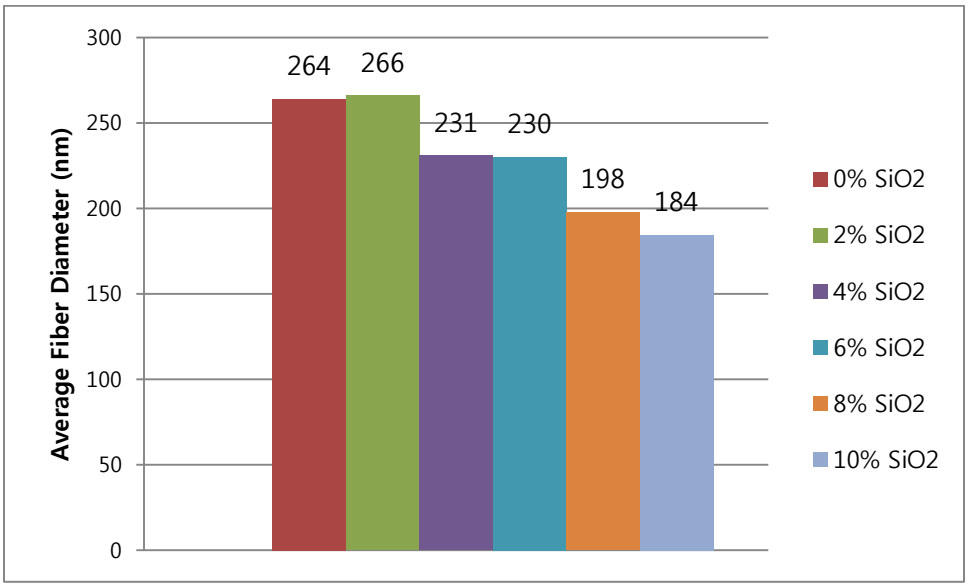

Figure 8. Average fiber diameter of different wt% of organosilicate P(VDF-TrFE) membranes.

6.1.2.2. TEM

TEM images were taken for visual confirmation of embedment of organosilicate nanoplates within the P(VDF-TrFE) nanofibers. Figure 9 are images of pure P(VDF-TrFE) membranes and 4 wt% organosilicate composite membranes. TEM images confirm the organosilicate nanoplates' embedment and alignment of organosilicate nanoplates can be seen. This alignment is due to the high extension of the electrospun jet. Organosilicate nanoplates are randomly oriented in the solution, and it gets aligned when solution is developed into the Taylor cone. Further directional alignment of organosilicate happens during elongation when jet travels [50].

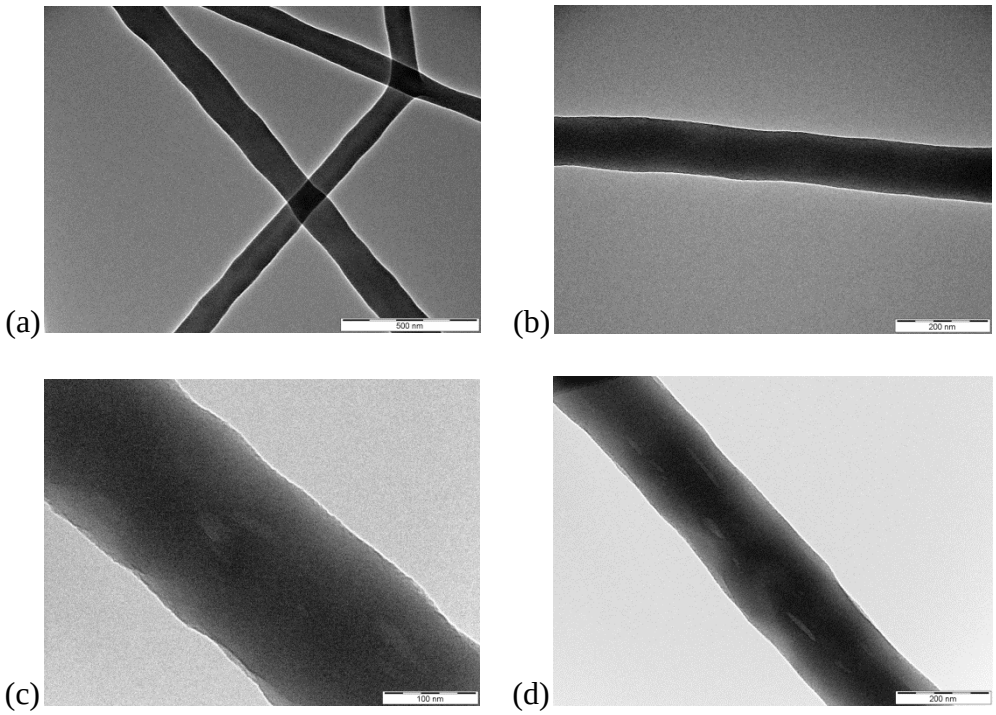

Figure 9. The TEM images of (a), (b) P(VDF-TrFE) membrans, and (c), (d) 4% SiO_2.

6.1.2.3. WAXD

Percent crystallinity (X_c) and crystallite size can be observed with WAXD data. All electrospun P(VDF-TrFE) membrane, and P(VDF-TrFE)/organosilicate composite membranes have a strong peak at 2 theta = 20.2°. This peak corresponds to the (220)/(110) lattice plane of the β phase crystallite. X_c values of composite membranes containing 2 wt%, 4 wt%, 6wt %, and 8 wt% organosilicate are higher than that of P(VDF-TrFE) membrane containing no organosilicate. However, 10 wt% organosilicate composite membrane's X_c value is lower than P(VDF-TrFE) membrane. Organosilicate may have nucleation effect to assist the crystallization of β phase. However, if there is too much, organosilicate could interference the crystallization by aggregated on its own.

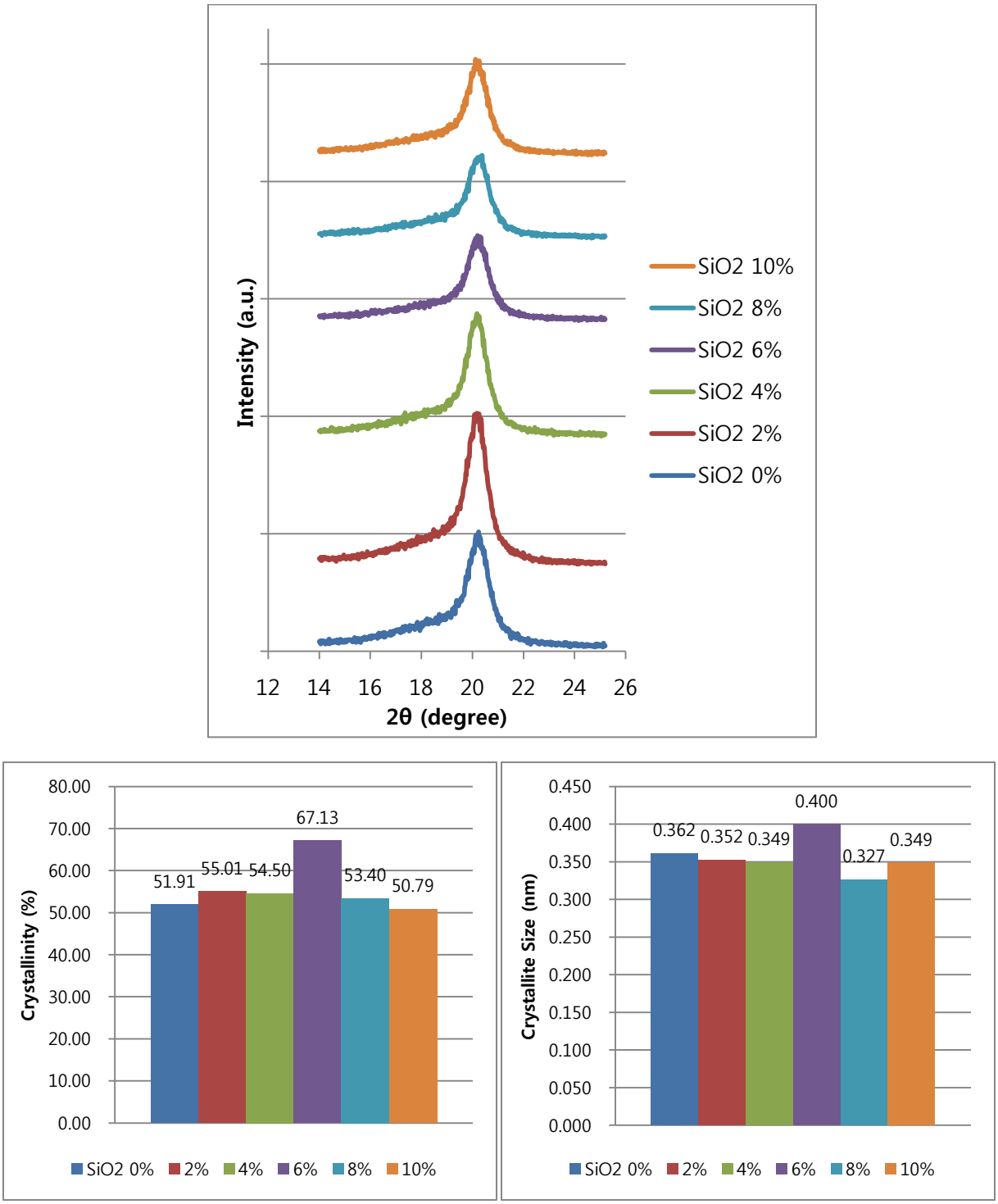

Figure 10. The WAXD patterns (top), analyzed percent crystallinity (bottom, left), and crystallite size (bottom, right).

Crystallite size (D) can be calculated using the Scherrer equation [51, 52].

$$D = \frac{K\lambda}{B\cos\theta} \quad (1)$$

In this equation, K is a dimensionless number of the order of unity, known as the Scherrer constant (0.9). λ is the X-ray wavelength, B is the full width at half-maximum of the diffraction peak in question (in 2θ), and θ is the peak angular position. $D_{220/110}$ at room temperature is shown in Figure 10. Most of organosilicate/P(VDF-TrFE) composite membranes have smaller crystallite sizes than P(VDF-TrFE) membrane. This has the opposite tendency to X_c. It is possible that organosilicate assists crystallization and results higher percentage of crystallinity (X_c) but smaller crystal sizes from shorter crystallization time involved.

6 wt% organosilicate/P(VDF-TrFE) composite membrane has exceptionally high X_c and $D_{220/110}$. From previous piezoelectric response analysis, it also had exceptionally high voltage output. Higher voltage output than rest of organosilicate/P(VDF-TrFE) samples can be explained from high X_c and $D_{220/110}$. However, the reason of the exceptionally high X_c and $D_{220/110}$ of the 6 wt% organosilicate/P(VDF-TrFE) composite membrane is uncertain.

Figure 11 shows three peaks between 0 to 10° in WAXD patterns which represent the organosilicate within membranes. Pure P(VDF-TrFE) membrane (viz. 0% SiO_2) does not have any peaks in this range while organosilicate composite membranes have clear peaks. Peak intensity increases as percentage of organosilicate increases.

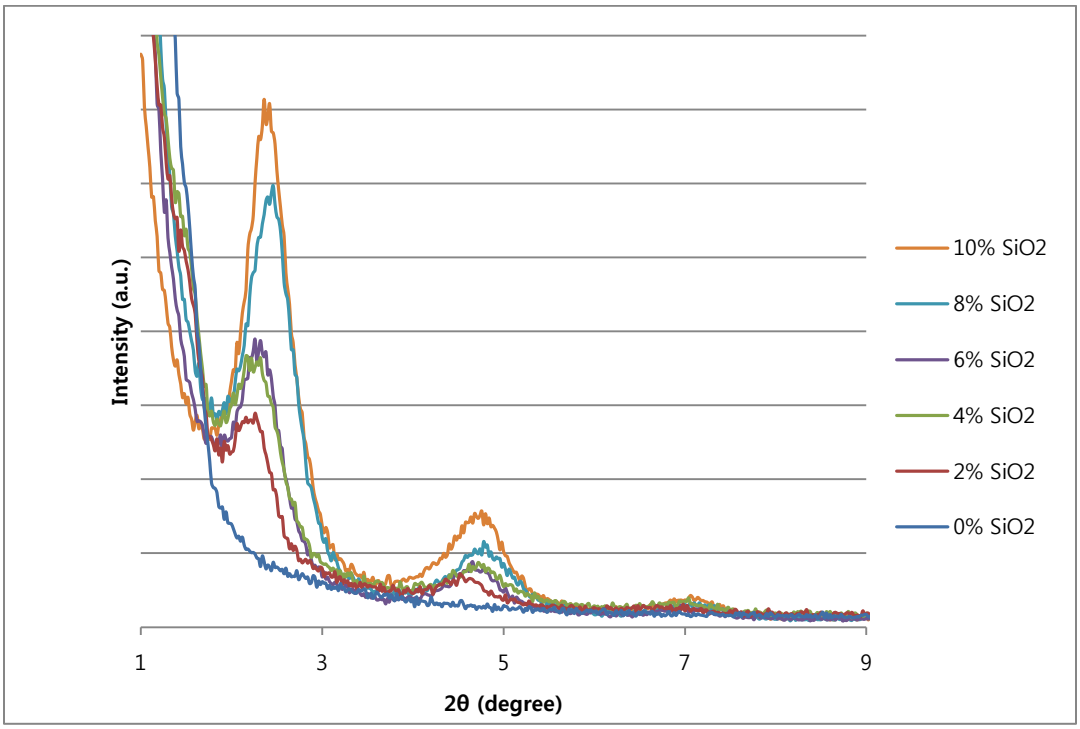

Figure 41. The WAXD patterns of electrospun membranes at low-angle range.

6.1.2.4. FTIR

Figure 12 is the FTIR spectra of electrospun P(VDF-TrFE) and organosilicate/P(VDF-TrFE) composite membranes. All membranes have clear β phase crystalline peaks indicating presence of organosilicate does not interfere with formation of β phase crystal of P(VDF-TrFE).

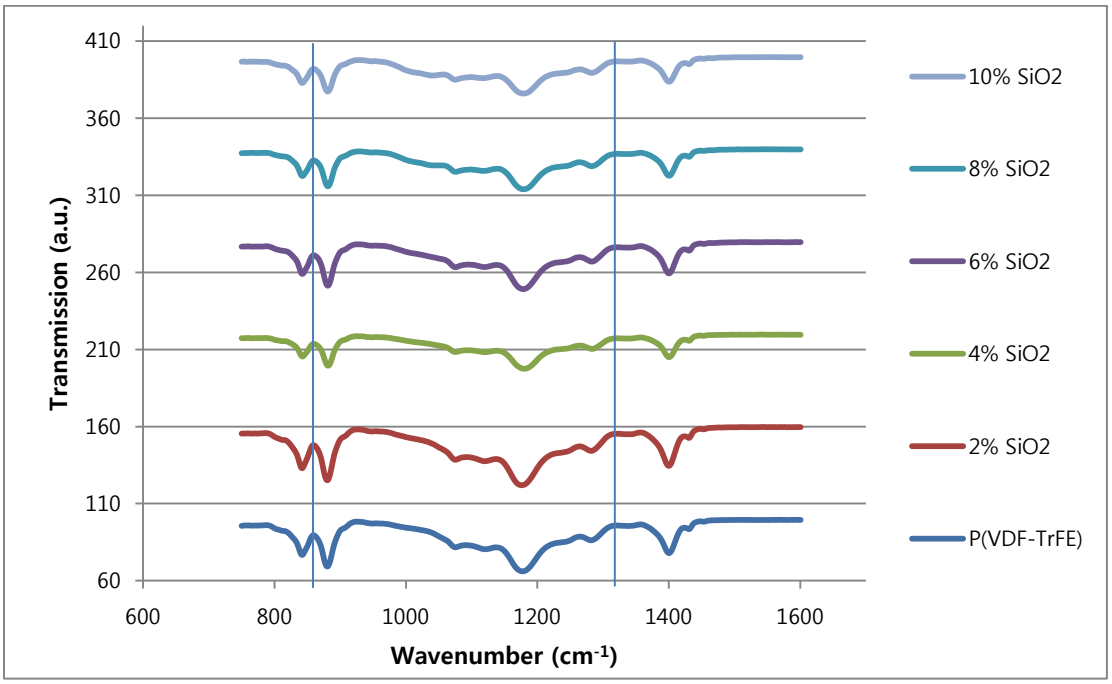

Figure 12. The FTIR spectra of electrospun P(VDF-TrFE) and organosilicate/P(VDF-TrFE) composite membranes.

In figure 13, two peaks at 1038 and 1007 cm^{-1} is indicated with β phase crystalline peaks. The two peaks ares from the Si-O stretching vibrations which confirms the integration of organosilicate into the organosilicate/P(VDF-TrFE) membranes.

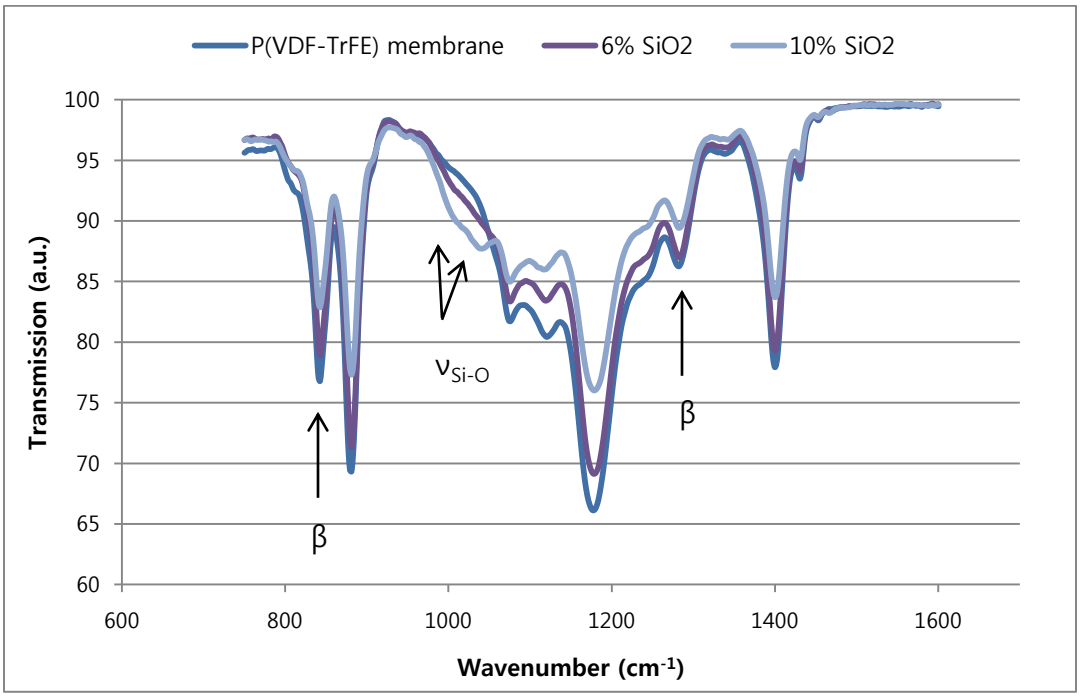

Figure 13. The FTIR spectra indicating Si-O stretching vibrations and β crystal phase.

6.1.2.5. DSC

For analysis of transitional behavior of the samples, a DSC measurement was conducted. Figure 14 and Table 1 summarizes the DSC results obtained from P(VDF-TrFE) membrane and organosilicate/P(VDF-TrFE) composite membranes. Ferroelectric property of P(VDF-TrFE) exhibits two endothermic peaks. The first peak at lower temperature 128℃ is due to ferroelectric to paraelectric (F-P) transition, while the second peak at higher temperture142℃ is due to the melting of crystals. F-P phase transition temperature T_c is around 128℃, and crystal melting temperature T_m is around 142℃. F-P transition peak represents successful formation of β crystals during electrospinning [53, 54].

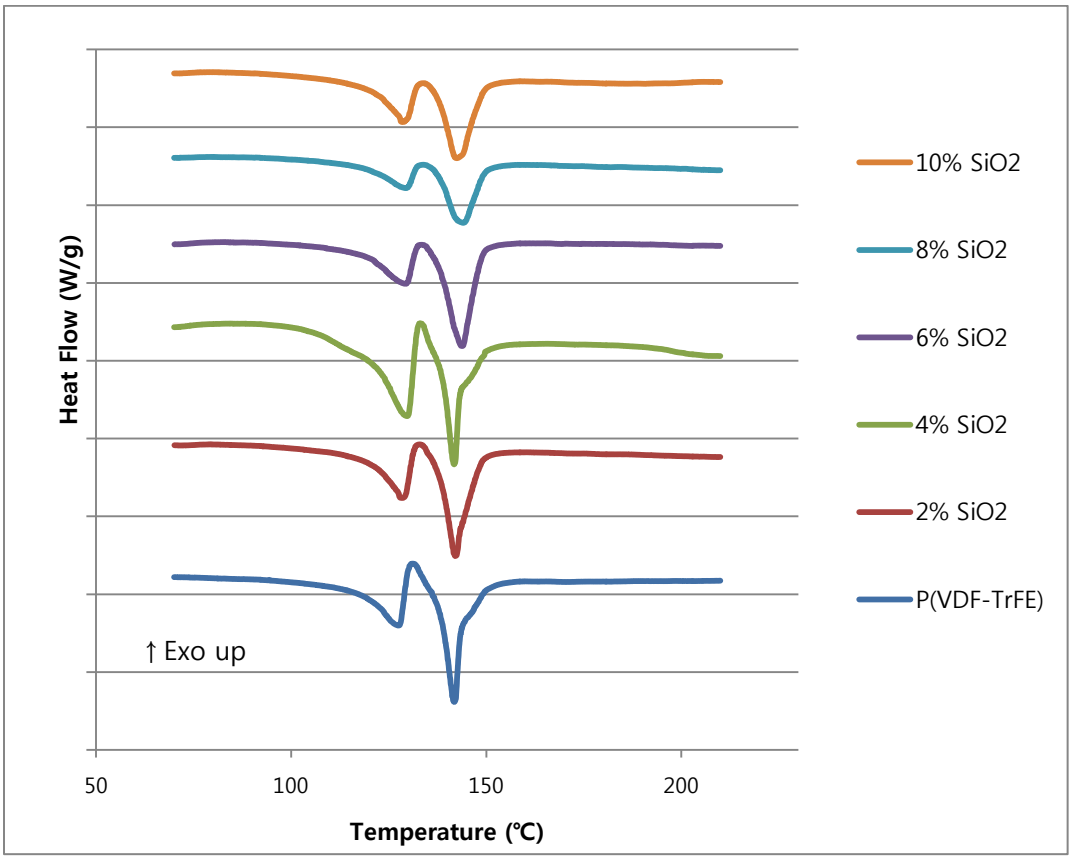

Figure 14. The DSC thermograms of P(VDF-TrFE) membrane and organosilicate/P(VDF-TrFE) composite membranes.

Sample	T_c (℃)	T_m (℃)	ΔH_c(J/g)	ΔH_m(J/g)
P(VDF-TrFE)	127.71	141.73	22.47	29.53
SiO_2 2%	128.55	141.94	17.53	26.55
SiO_2 4%	129.75	141.77	35.55	24.71
SiO_2 6%	129.37	143.82	15.34	26.76
SiO_2 8%	129.24	144.14	13.92	24.15
SiO_2 10%	128.43	142.47	13.96	21.00

Table 1. DSC data of F-P transition temperature T_c, melting temperature T_m, phase transition enthalpy ΔH_c, and melting enthalpy ΔH_m dependence of organosilicate wt% for P(VDF-TrFE) membranes.

6.1.2.6. Membrane Density and Breathability

The densities of electrospun P(VDF-TrFE) membrane and organosilicate/P(VDF-TrFE) composite membranes are calculated in Table 2. Densities of electrospun membranes are about 24% of the density of bulk P(VDF-TrFE), 1.85g/cm^3. Porosity can be calculated from

$$Porosity(\%) = [1 - \frac{Density_{membrane}}{Density_{polymer}}] \times 100 \quad (2)$$

The calculated porosity of electrospun membranes is in the range of 74-77%. Organosilicate have very little effect on the membrane structure, porosity, therefore also have very little effect on the breathability of the membranes. This can be further confirmed with the water vapor transmission rates (WVTRs).

Sample	Membrane density (g/cm^3)	Porosity (%)	WVTRs [(g/hour·m^2)]
P(VDF-TrFE)	0.48	74.0	16.8
SiO_2 2%	0.44	76.2	17.7
SiO_2 4%	0.43	77.0	15.1
SiO_2 6%	0.43	76.7	16.4
SiO_2 8%	0.46	75.1	17.1
SiO_2 10%	0.43	76.8	17.1

Table 2. Values of density, porosity, and WVTRs of electrospun membranes.

6.1.2.7. Tensile Test

The results of tensile test are listed in Table 4. Pure P(VDF-TrFE) membrane's weak

mechanical properties improved significantly with addition of organosilicate. Young's modulus obtained from the stress-strain graph of P(VDF-TrFE) membrane is 5.99±2.05 MPa. The modulus of organosilicate composite membranes were 312~448% of pure P(VDF-TrFe) membrane, 18.69~26.82 MPa. Young's modulus increased as the percentage of organosilicate in the composite membrane increased. Tensile strength of P(VDF-TrFE) was 1.33±0.16 MPa while organosilicate composite membranes were 12.89~21.51 MPa which is 969~1617% improvement. Elongation at break also increased as well, showing 126~200% enhancement. P(VDF-TrFE) elongated 55.11±6.28 at break and organosilicate composite membranes elongated 69.32~110.09%. Weak P(VDF-TrFE) membrane, toughness of 0.47±0.08 J/m^3, became tougher by addition of organosilicate exhibiting toughness of 6.39~9.69 J/m^3 which is 1360~2062% advancement.

Sample	Young's modulus (MPa)	Tensile strength (MPa)	Elongation at break (%)	Toughness (J/m^3)
P(VDF-TrFE)	5.99±2.05	1.33±0.16	55.11±6.28	0.47±0.08
SiO_2 2%	18.69±1.69	21.51±1.72	84.59±7.56	9.69±1.79
SiO_2 4%	22.40±2.31	13.03±1.11	110.09±13.85	9.20±1.83
SiO_2 6%	23.17±3.41	19.92±0.95	73.25±4.65	7.76±0.89
SiO_2 8%	24.75±2.32	17.95±0.90	69.32±4.11	6.39±0.72
SiO_2 10%	26.82±3.81	12.89±1.18	89.59±10.45	7.13±0.74

Table 3. Values of Young's modulus, tensile stregth, elongation at break, and toughness for electrospun membranes.

6.2. Effect of Fiber Orientation in Membranes

6.2.1. Piezoelectric Response

The piezoelectric responses of PVDF-TrFE membranes' with different fiber orientations were measured with a customized equipment consisting of the compression mode of Instron 5566 and Fluke 8846A digital multimeter combined with a lab charge amplifier in a charge output mode (10nF). A compressive pressure of 0.07 MPa (corresponding to the human foot pressure range of 0-0.20MPa [49]) was applied in the experiments. As can be seen from Figure 15, the variation (as shown by the standard deviation in the graph) of the voltage measurement is sometimes very large. Nevertheless, it can observed that, with the increase of the rotation speed of the collector, which should correspond to improved fiber alignment in the membrane, voltage output generally increases except for P(VDF-TrFE) membrane collected with rotator speed 2000rpm. This may be due to the large variation of the coherency of the fiber alignment in the P(VDF-TrFE) membrane collected with rotator speed 2000rpm which will be shortly discussed.

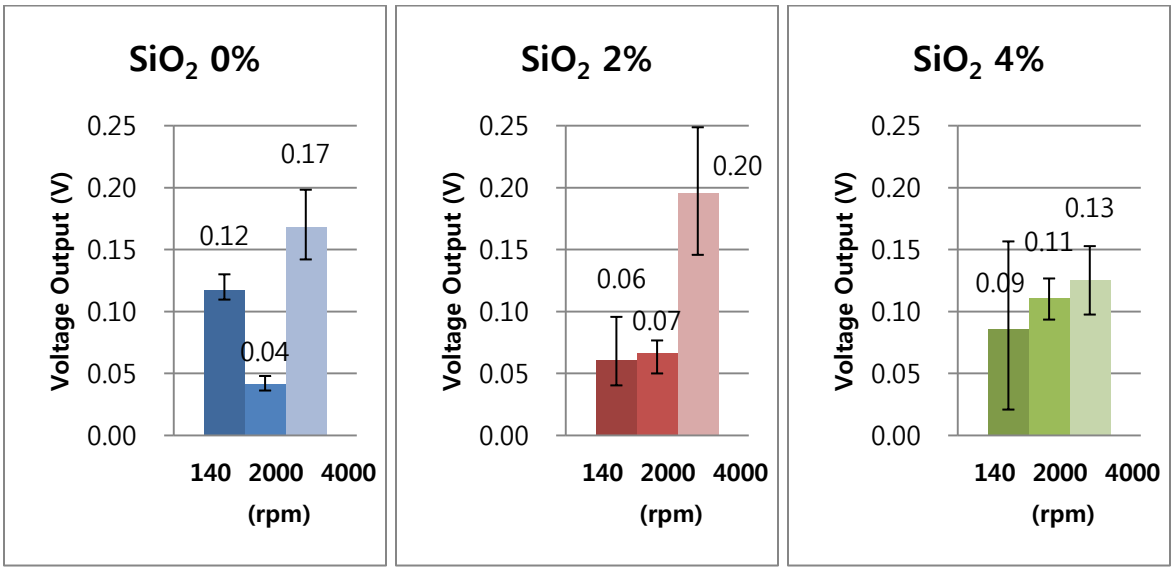

Figure 15. Voltage output of different fiber orientation membranes with different organosilicate wt% (From left to right, SiO_2 0%, SiO_2 2%, SiO_2 4%).

6.2.2. Fiber and Membrane Characterizations

6.2.2.1. SEM

6.2.2.1.1. Fiber Orientation

From SEM images, the fiber orientation of the membrane samples were evaluated by OrientationJ, plug-in of ImageJ, image processing and analysis Java program. Quantitative and distribution of the fiber orientation was evaluated utilizing OrientationJ. Quantitative measurements provide orientation angle and coherency of the orientation within the region of interest. The distribution of the orientation is evaluated by the structure tensor of every pixel of the image. The distribution histogram is a weighted histogram; the weight is the coherency itself [44].

Figure 16 shows how original image (left, top) is analyzed. The orientation angle and coherency is analyzed within region of interest (right, top). The distribution of the orientation obtained from analysis of the structure tensor of every pixel image (left, bottom) and the distribution histogram from it (right, bottom).

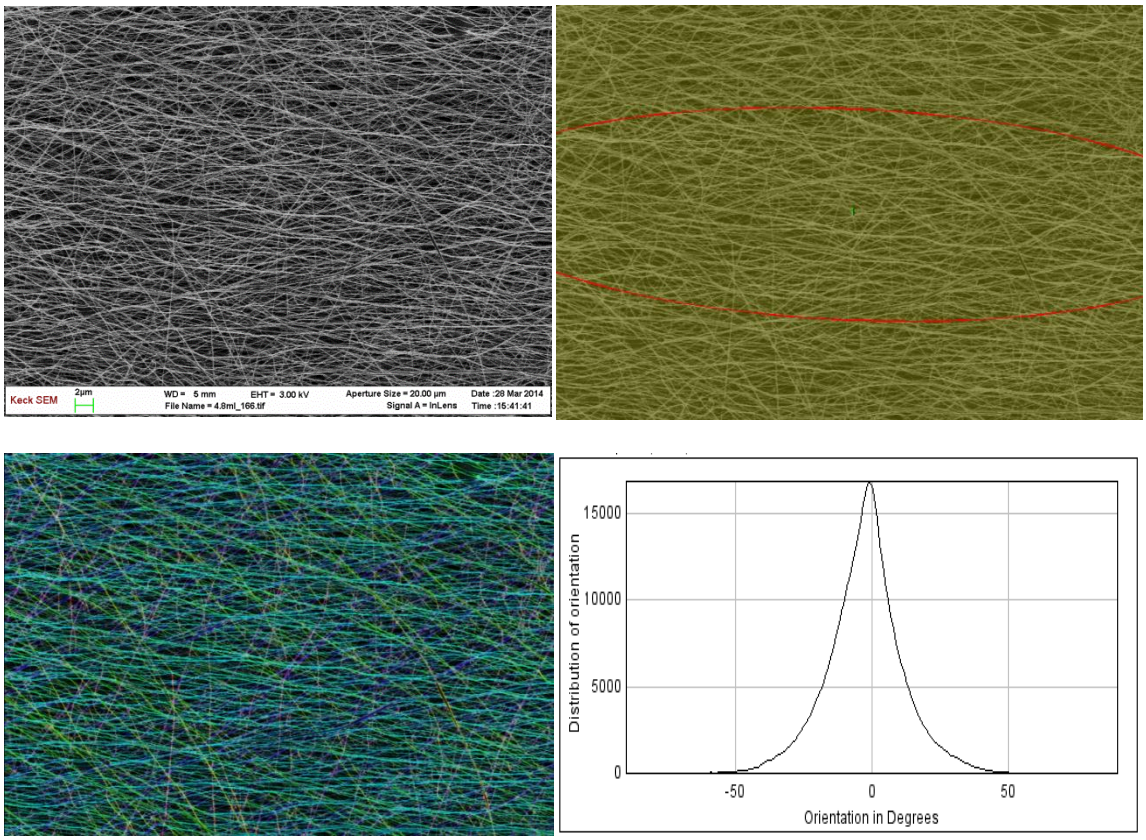

Figure 16. SiO_2 4%, 2000rpm image analysis.

Fiber orientation coherencies from the quantitative measurements can be seen in the Figure 17. Samples fabricated with faster rotating speed of the collector (viz. 2000rpm and 4000rpm) generally had higher fiber orientation coherency than samples fabricated with slower rotating collector samples (viz. 140rpm). However, between 2000rpm and 4000rpm collector speed, fiber orientation did not improve significantly. There seems an interaction between the rotation speed of collector and weight percentage of organosilicate on fiber orientation, perhaps because the add-on of organosilicate changed the dielectric property of the polymer solution and fibers spun.

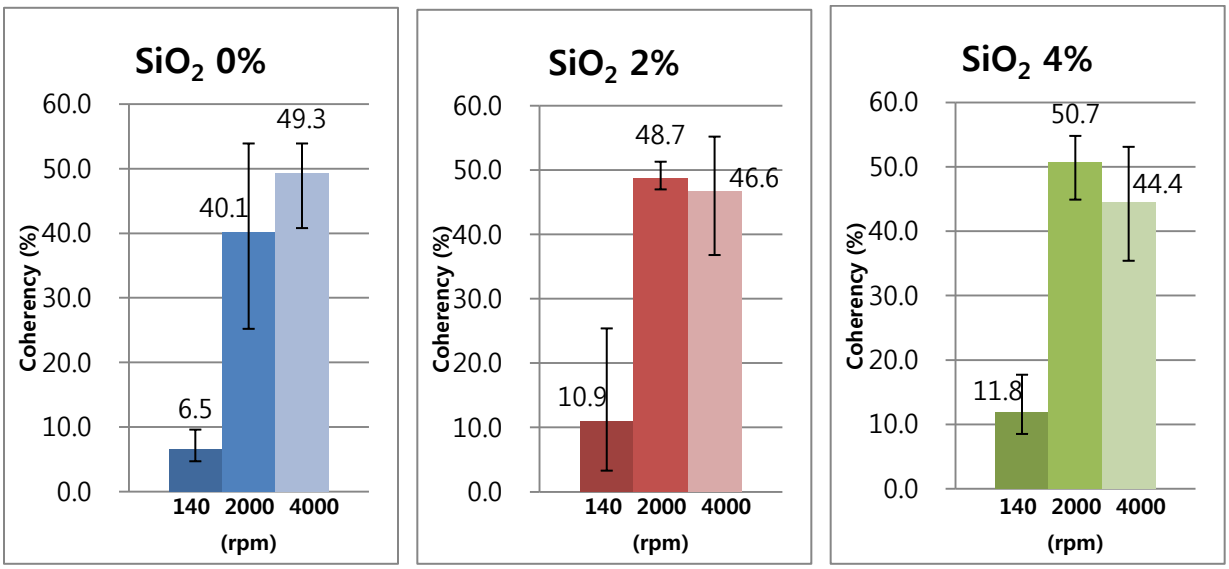

Figure 17. The fiber orientation coherency comparison within the same organosilicate composite percentage: SiO_2 0% (left), SiO_2 2% (middle), and SiO_2 4% (right).

6.2.2.1.2. Influence of Fiber Orientation and Organosilicate on Voltage Output

Table 4 is the result of analysis of variance (ANOVA) of organosilicate (SiO_2), and collector rotation speed (rpm) on voltage output. Collector rotation speed (rpm), and interaction of organosilicate and collector rotation speed (SiO_2*rpm) have significant influence on voltage output (Sig.<0.05). However, SiO_2 does not have significance on voltage output (Sig. >0.05).

Tests of Between-Subjects Effects

Dependent Variable: VoltageOutput

Source	Type III Sum of Squares	df	Mean Square	F	Sig.
Corrected Model	.062[a]	8	.008	6.661	.000
Intercept	.315	1	.315	271.579	.000
SiO_2	1.238E-5	2	6.188E-6	.005	.995
rpm	.042	2	.021	18.184	.000
SiO_2 * rpm	.020	4	.005	4.228	.014
Error	.021	18	.001		
Total	.397	27			
Corrected Total	.083	26			

a. R Squared = .748 (Adjusted R Squared = .635)

Table 4. ANOVA analysis of organosilicate (SiO_2), and collector rotation speed (rpm) on voltage output.

6.2.2.1.3. Fiber Diameter

The fiber diameters of the membrane samples were evaluated by the mean of more than 50 measurements. Figure 18 shows the fiber diameter measurements. Collector rotation speed did not have significant influence fiber diameters. Electrospun fibers solidify fast after leaving the trajectory, and thus did not get extra stretching effect from fast rotating collector. Most of P(VDF-TrFE)/organosilicate composite membranes have finer fibers than pure P(VDF-TrFE) membranes which was also reported in other studies. Enhanced electrical conductivity of the electrospinning solution containing organosilicate results finer fibers [45-47].

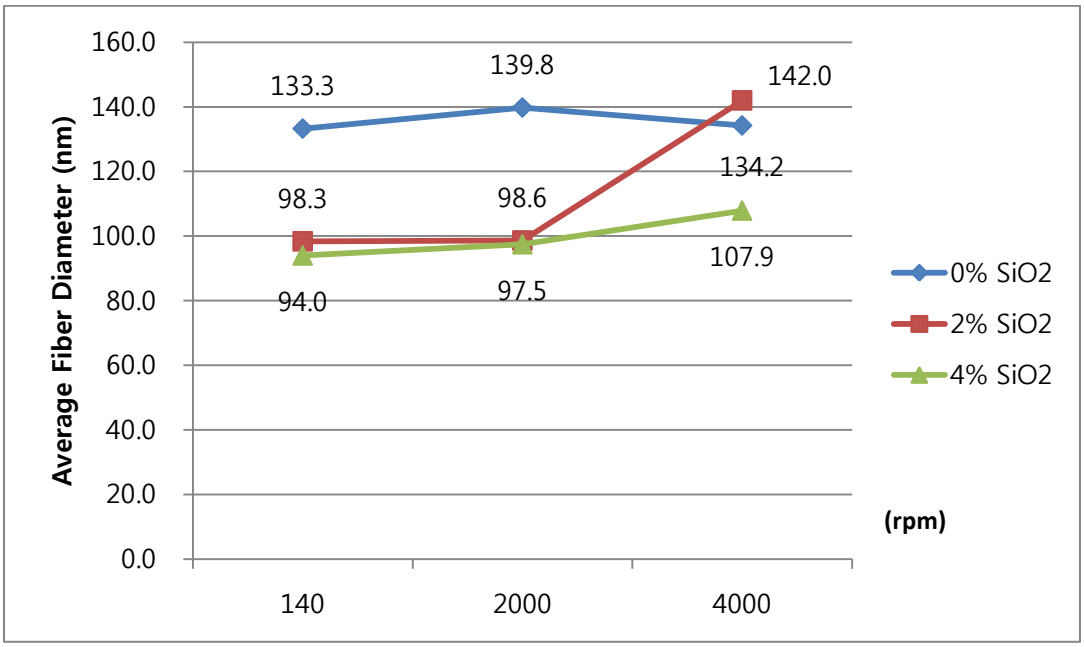

Figure 18. Average fiber diameter of electospun membranes with different SiO_2 percentage and collecting speed.

6.2.2.2. WAXD

All electrospun P(VDF-TrFE) membranes with different SiO_2 percentage and collecting speed have a strong peak at 2 theta = 20.2°. This peak corresponds to the (220)/(110) lattice plane of the β phase crystallite. Observing WAXD patterns in Figure 19, peak intensity at 20.2° (2θ) increases as collecting speed increases with P(VDF-TrFE) membranes, 0% SiO_2. For 2% and 4% SiO_2 membranes, lowest collecting speed (viz. 140rpm) have the higher peak intensity at 20.2° (2θ) than higher collecting speeds (viz. 2000rpm and 4000rpm).

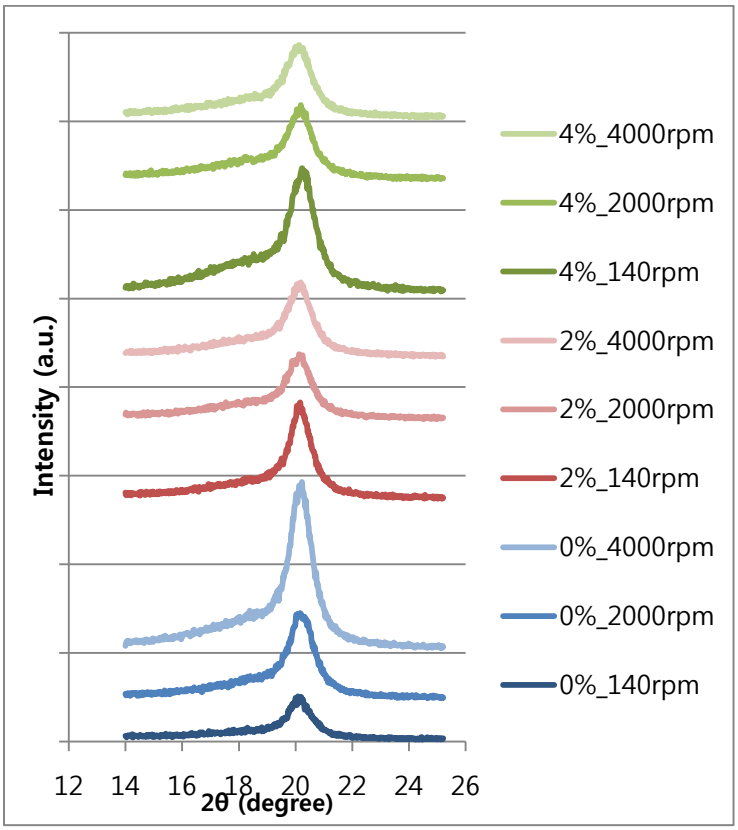

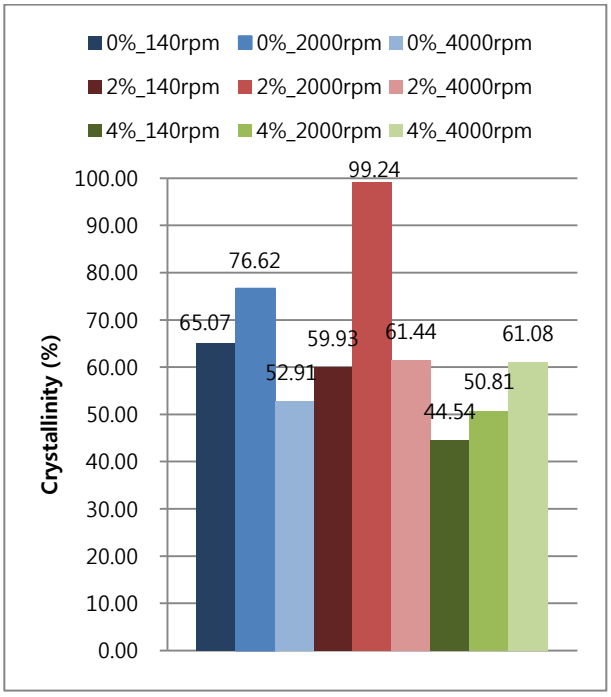

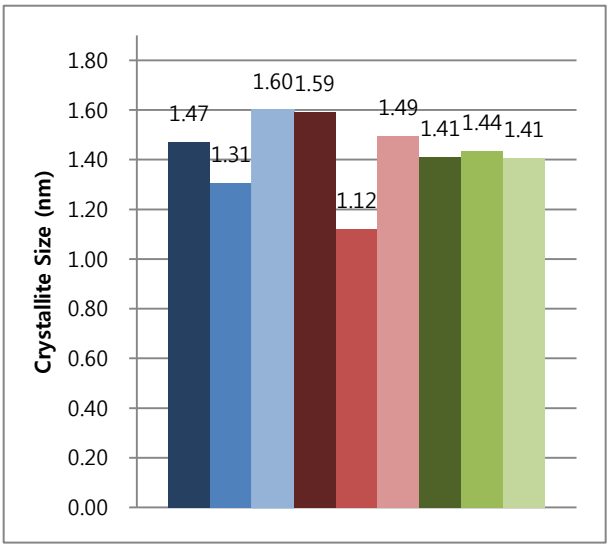

Figure 19. The WAXD patterns of electrospun membranes with different SiO_2 percentages and collecting speeds (top). Percent crystallinity (bottom, left), and crystallite size (bottom, right) an alyzed from WAXD results.

Percent crystallinity (X_c) can be analyzed from WAXD data using Jade program. The full width at half-maximum of the diffraction peak in 2θ can be also obtained by WAXD pattern analysis. With this data, Crystallite size (D) can be calculated using the Scherrer equation [51, 52].

$$D = \frac{K\lambda}{B\cos\theta} \tag{1}$$

In this equation, K is a dimensionless number of the order of unity, known as the Scherrer constant (0.9). λ is the X-ray wavelength, B is the full width at half-maximum of the diffraction peak in question (in 2θ), and θ is the peak angular position. $D_{220/110}$ at room temperature is shown in Figure 19. P(VDF-TrFE) membrane and 2% SiO_2 membrane collected at 2000rpm shows exceptionally small crystallite size. Smaller crystallite size could be the reason for the low voltage output of P(VDF-TrFE) and 2% SiO_2 membrane collected at 2000rpm regardless of high crystallinity.

Incorporation of organosilicate can be seen in the low-angle range of WAXD patterns in Figure 20. Three peaks in the range of 0~10° represents the successful incorporation of organosilicate into P(VDF-TrFE) membranes.

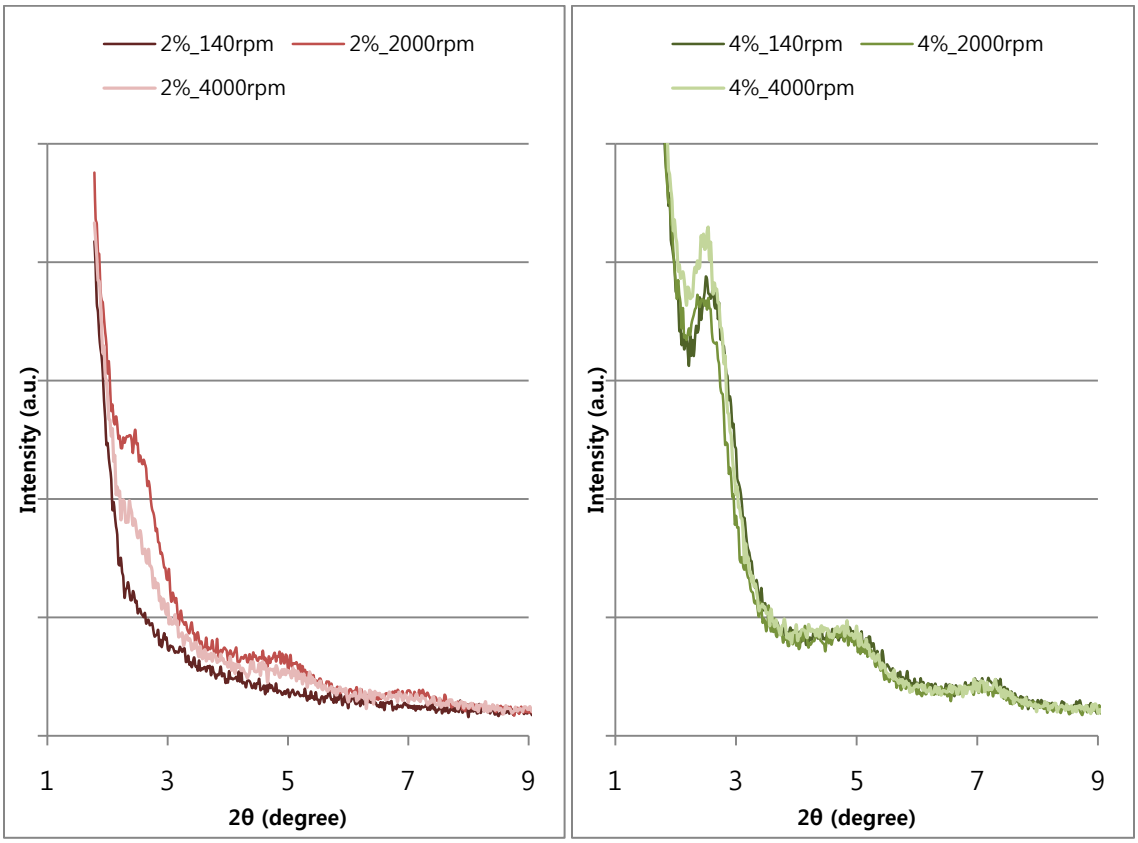

Figure 20. The WAXD patterns of electrospun membranes with different collecting speeds. 2% SiO_2 (left), and 4% SiO_2 (right).

6.2.2.3. FTIR

Figure 21 is the FTIR spectra of electrospun P(VDF-TrFE) membranes with different SiO2 percentages and collecting speeds. All membranes have clear β phase crystalline peaks at 1038 and 1007 cm^{-1}. Peak intensity is similar at 1038 cm^{-1} but difference can be seen at 1007 cm^{-1}. For P(VDF-TrFE) membranes, there is a clear tendency of higher peak for higher collector rotation speed. However, this tendency cannot be seen with 2% SiO_2 or 4% SiO_2 membranes which coincides with the WAXD peak intensity at 20.2°(2θ).

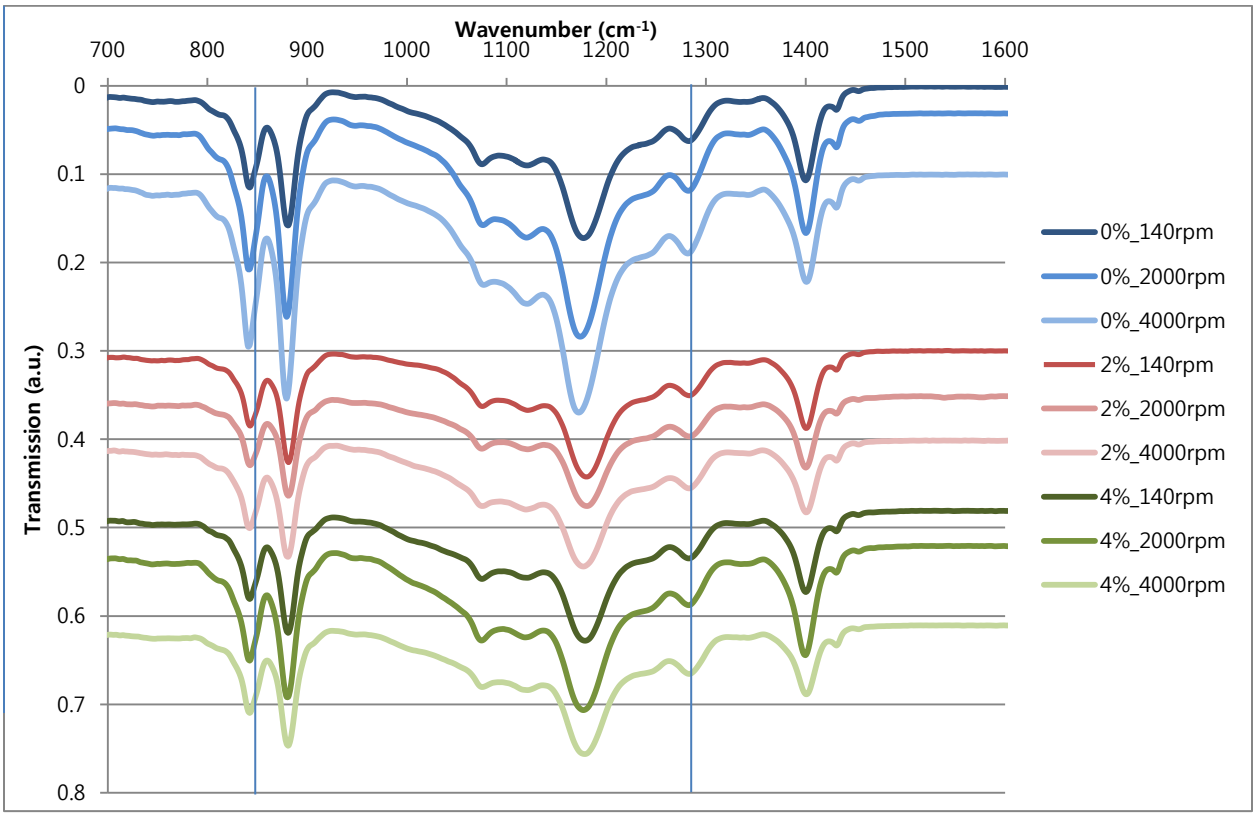

Figure 21. The FTIR spectra of electospun P(VDF-TrFE) membranes with different SiO_2 percentages and collecting speeds.

6.2.2.4. DSC

Table 5 and Figure 22 summarizes the DSC results obtained from P(VDF-TrFE) membrane and organosilicate/P(VDF-TrFE) composite membranes. Ferroelectric property of P(VDF-TrFE) exhibits two endothermic peaks. The first peak at lower temperature 128℃ is due to ferroelectric to paraelectric (F-P) transition, while the second peak at higher temperture143℃ is due to the melting of crystals. F-P phase transition temperature T_c is around 128℃, and crystal melting temperature T_m is around 142℃. F-P transition peak represent successful formation of β crystals during electrospinning [53, 54].

	T_c (℃)	T_m (℃)	ΔH_c(J/g)	ΔH_m(J/g)
SiO_2 0%_140rpm	129.09	142.15	18.23	26.76
2000rpm	127.56	143.91	10.12	20.02
4000rpm	127.50	144.53	14.29	29.96
SiO_2 2%_140rpm	127.55	143.71	14.62	30.69
2000rpm	128.59	142.75	16.11	28.43
4000rpm	129.06	142.28	19.57	29.00
SiO_2 4%_140rpm	128.25	142.28	17.38	26.58
2000rpm	128.87	142.29	21.09	29.51
4000rpm	128.77	142.26	16.83	27.47

Table 5. DSC data of F-P transition temperature T_c, melting temperature T_m, phase transition enthalpy ΔH_c, and melting enthalpy ΔH_m dependence of electrospun membranes with different organosilicate percentage and collecting speeds.

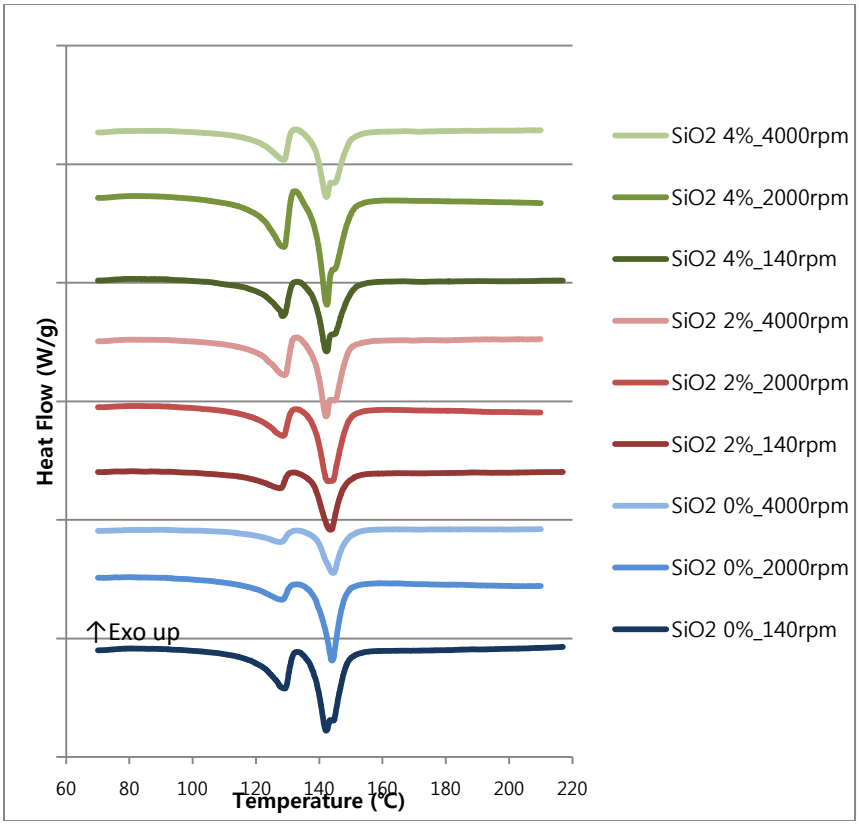

Figure 52. The DSC thermograms of electrospun membranes with different organosilicate percentage and collecting speeds.

6.2.2.5. Tensile Test

Tensile testing results are listed in Table 6 and Figure 23. All samples were tested in width (W) and length (L) direction. Longitudinal direction is the direction of the collector rotation direction, thus the direction of the fiber alignment. For pure P(VDF-TrFE) membranes, Young's modulus, tensile strength, and toughness of the membrane in the fiber alignment direction (L) increases as collecting speed increases. As collecting speed increases, elongation at break decreases in the fiber alignment direction (L), however it increases in the width direction (W). Young's modulus, tensile strength, and toughness of the membrane in the width direction (W) decreases as collecting speed increases. Organosilicate composite membranes' mechanical properties according to the fiber collecting speed does not have significant difference as the pure P(VDF-TrFE) membranes. Tensile strength of the faster collecting speed samples (viz. 2000rpm and 4000rpm) in the fiber alignment direction (L) is higher than slow collecting speed (viz. 140rpm).

Direction	Sample	Young's modulus (MPa)	Tensile strength (MPa)	Elongation at break (%)	Toughness (J/m^3)
Width	SiO_2 0%_140rpm	89.09±39.96	5.51±2.40	20.94±6.75	3.51±3.14
	2000rpm	29.24±5.99	4.16±0.44	58.45±5.54	13.93±3.15
	4000rpm	17.56±4.72	4.07±0.44	112.72±17.98	62.01±27.07
	SiO_2 2%_140rpm	72.15±25.42	5.96±2.35	26.56±6.86	4.60±3.69
	2000rpm	23.39±19.60	1.57±0.55	30.82±8.24	2.26±1.16
	4000rpm	14.33±7.87	4.60±5.94	101.79±6.44	57.10±6.45
	SiO_2 4%_140rpm	39.87±17.39	17.73±0.33	46.81±3.54	45.82±11.22
	2000rpm	21.17±8.39	4.30±0.95	44.22±4.98	10.22±5.30
	4000rpm	24.91±4.29	6.25±0.08	87.02±1.15	55.04±1.56
Length	SiO_2 0%_140rpm	84.48±11.56	17.78±0.72	67.96±5.22	108.49±24.92
	2000rpm	178.08±34.35	31.16±5.05	47.42±8.00	111.88±36.49
	4000rpm	279.44±117.83	35.14±4.36	43.96±11.03	169.74±37.42
	SiO_2 2%_140rpm	74.73±19.75	13.19±0.61	67.34±1.92	70.14±5.03
	2000rpm	101.71±9.09	38.00±4.55	35.14±2.12	73.48±23.15
	4000rpm	34.87±24.55	24.61±10.75	34.55±5.87	33.57±16.56
	SiO_2 4%_140rp	37.47±12.17	14.46±2.31	59.66±11.21	51.12±20.34
	2000rpm	123.20±161.92	30.11±1.66	36.62±4.92	51.80±35.00
	4000rpm	146.20±88.44	22.71±14.92	36.15±7.08	49.86±42.46

Table 6. Results of tensile testing: Young's modulus, tensile strength, elongation at break, and toughness.

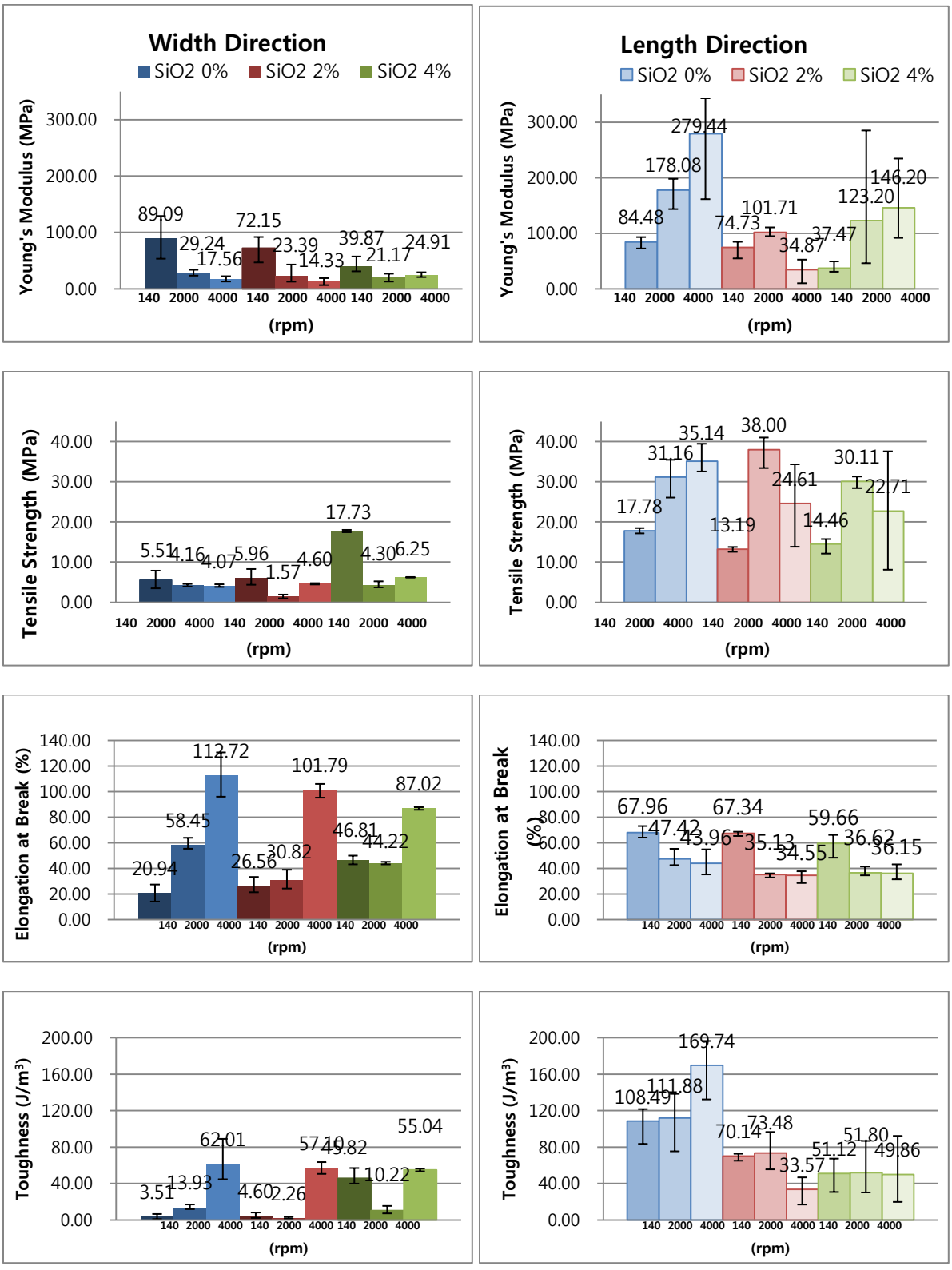

Figure 26. Young's modulus (top), tensile strength (2nd), elongation at break (3rd), and toughness (bottom).

6.3. Smart Shoe Prototype

A sports shoe was instrumented with the developed piezoelectric membrane sensor and a transceiver to demonstrate the possibility of monitoring foot pressure and body activities.

6.3.1. Components of Smart Shoe Prototype

For the wireless smart shoe prototype, a piezoelectric membrane sensor, which was made of the developed piezoelectric P(VDF-TrFE) membrane sandwiched by two layers of Aluminum foils as electrodes (See Fig. 24), was attached to the shoe sole (See Fig. 25) and the sensor was connected to a microcontroller (MSP430 from Texas Instruments) and a transceiver (CC2500 from Texas Instruments).

MSP430 is an Ultra-Low Power 16-bit microcontroller (MCU). The electric current drawn in idle mode can be less than 1 μA. The top CPU speed is 25 MHz. The MSP430 also uses six different low-power modes, which can disable unneeded clocks and CPU. Additionally, the MSP430 is capable of wake-up times below 1 microsecond, allowing the microcontroller to stay in sleep mode longer, minimizing its average current consumption. CC2500 is a low-cost 2.4 GHz transceiver designed for very low-power wireless applications. The circuit is intended for the 2400-2483.5 MHz ISM (Industrial, Scientific and Medical) and SRD (Short Range Device) frequency band.

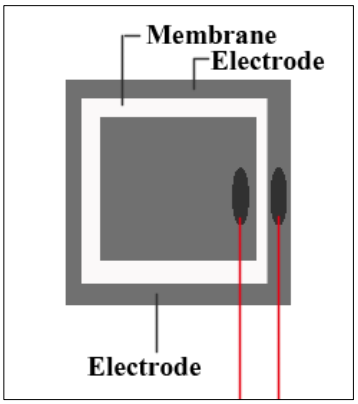

Figure 24. Diagram of the piezoelectric membrane sensor.

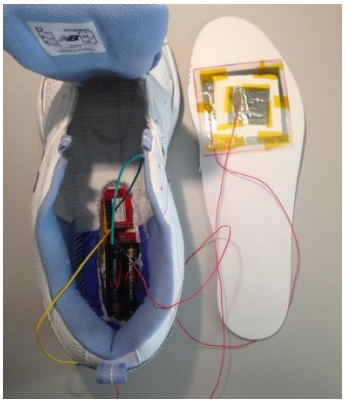

Figure 25. The piezoelectric membrane sensor connected to the battery board of the eZ430-FR2500.

The system was developed using eZ430-RF2500, which is a complete wireless development tool for the MSP430 and CC2500 that includes all the hardware and software required to develop an entire wireless project with the MSP430 in a convenient USB stick. The sensor was connected to the battery board of the eZ430-FR2500, as shown in the Figure 25, which transmits data to the target board wirelessly, and the target board transmits data to the personal computer (PC) by a USB port. The target board is powered through the USB port. Figure 26 is the block diagram of the connected components (top), and illustration (bottom).

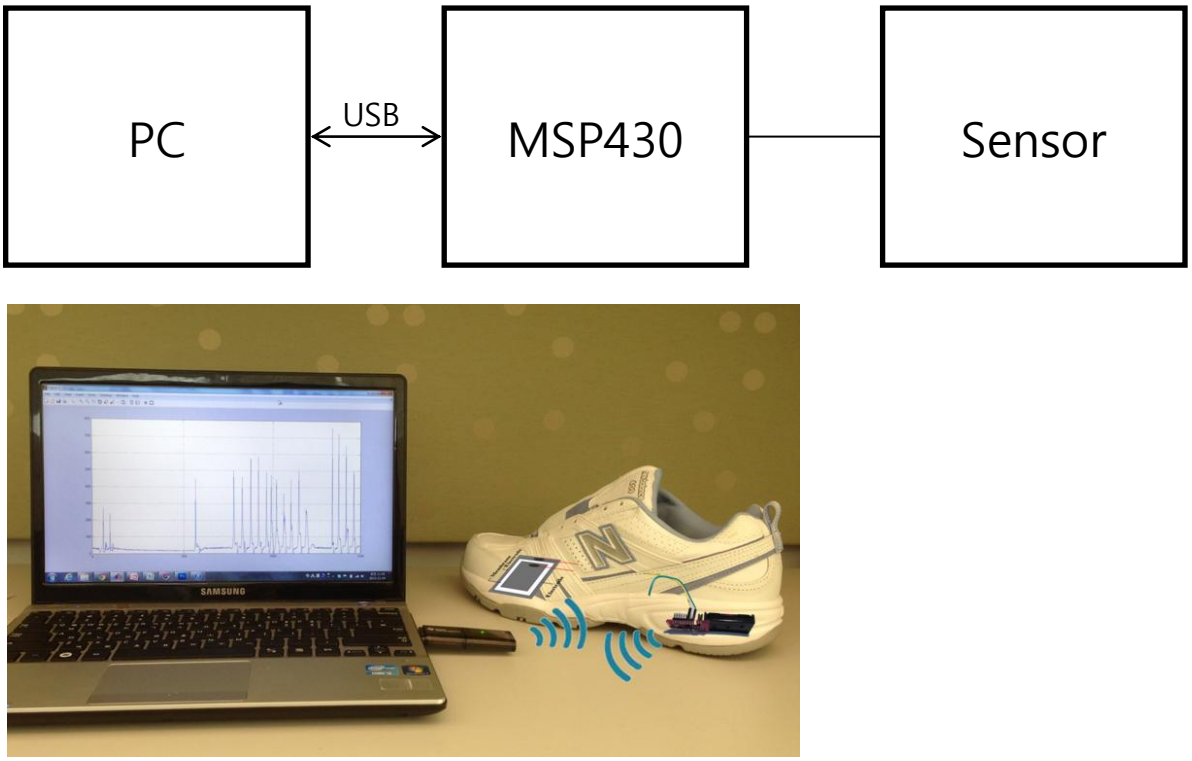

Figure 27. The block diagram of the smart shoe prototype (top), and the illustration (bottom).

6.3.2. Data Acquisition from the Smart Shoe Prototype

The instrumented shoe successfully transmitted the piezoelectric signals from the membrane sensor to the PC. Figure 27 shows an example of the signal acquired on the PC from the tapping motion on the smart shoe prototype. Clear peaks are visible from the input pressure and the recovery time was 2~3 seconds.

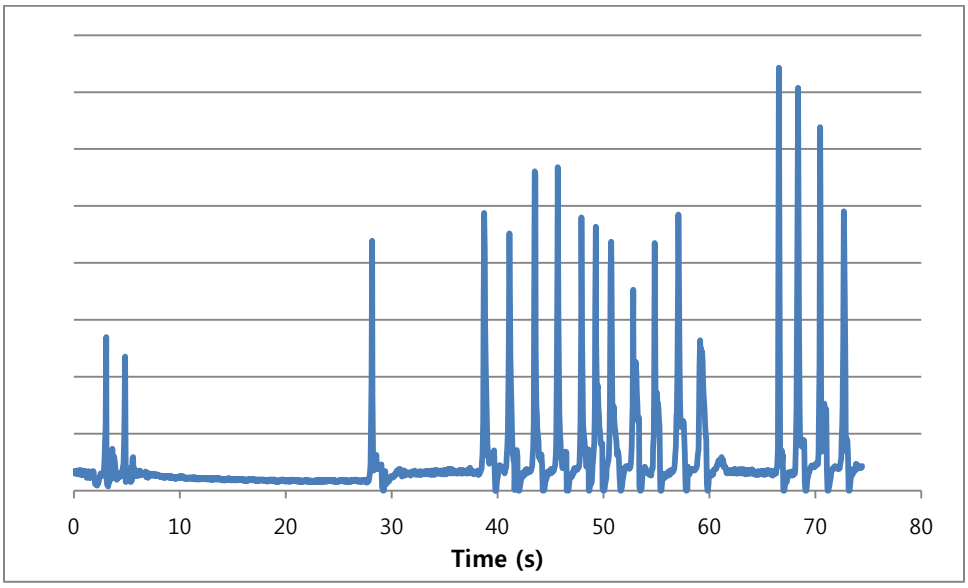

Figure 28. Data acquisition by tapping motion from smart shoe prototype.

In order to convert the electrical signal into pressure measurements, a relationship between the actual pressure and the signal strength should first be established. To do so, a 1 kg weight weight was placed on the sensor repeatedly to see whether a consistent signal can be obtained. Figure 28 plots the results. As can been seen, although input weight (viz. pressure) was constant, output signal intensity varies greatly.

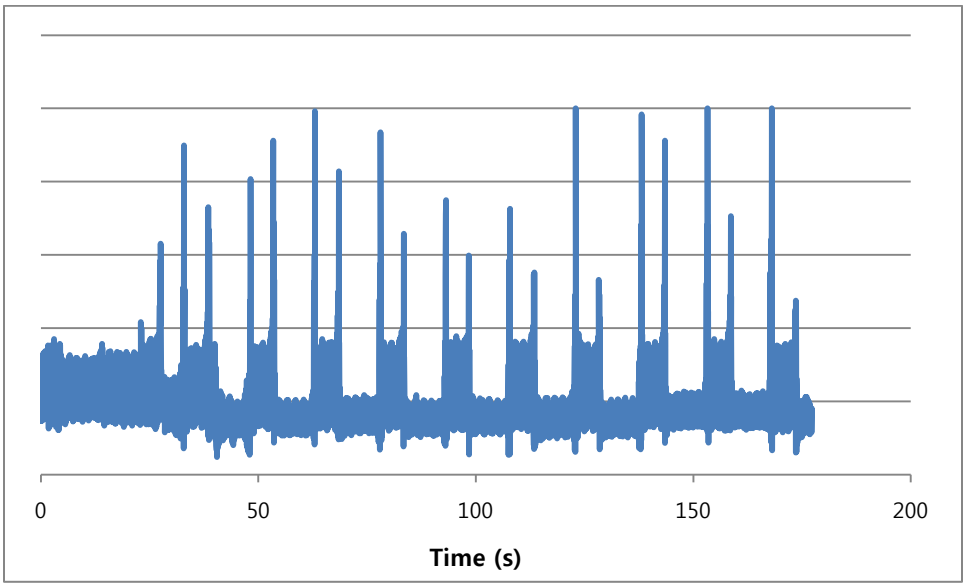

Figure 29. Data acquisition by placing 1 kg of weight on the sensor multiple times.

Inconsistency of signal intensity was also evident when 1 kg weight was placed on the sensor as a base, and a 200 g and 500 g weight were then placed on the top of the 1 kg weight alternatively. However, as shown in Figure 29, the signal intensity does not change in response to the changes in weight. This may be caused by the poor interfacial contacts between the piezoelectric membrane and Aluminum foil electrodes and the drifting of charges over time. Further work is required to identify the problem. The charge drifting problem may be solved by a technique developed in Professor Kan's lab in which the sensor works as an acoustic wave resonator in quasi-static pressure [55].

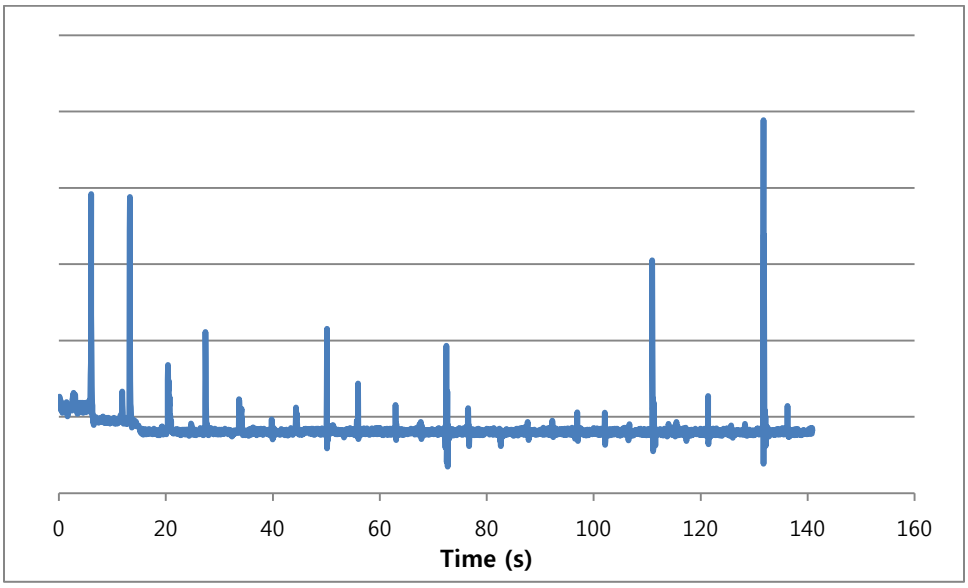

Figure 210. Plot of 1 kg weight was place on the sensor as a platform, and 200 g and 500 g weight placed on and off.

7. Conclusions

One objective of the this study was to improve the piezoelectric responses of electrospun P(VDF-TrFE)/ organosilicate fibrous membrane. By investigating the piezoelectric responses of P(VDF-TrFE)/ organosilicate fibrous membrane containing varying percentage of organosilicate, it was found that the composite membranes containing 6 wt% organosilicate had exceptionally high voltage output. WAXD results showed it had higher crystallinity and bigger crystallite size than other P(VDF-TrFE)/ organosilicate composite membrane. By further examining the piezoelectric responses, crystallinity and crystallite size of electrospun membranes fabricated at varying drum collector speeds, it was found that higher piezoelectric response is associated with bigger crystallite size, not the percentage of crystallinity.

From measuring the piezoelectric responses of electrospun P(VDF-TrFE)/ organosilicate fibrous membrane fabricated at different drum collector rotation speeds, it was found there is a tendency that the piezoelectric response increases with increasing rotation speed, which may be a combined result of enhanced fiber orientation in the membrane and an increase in crystallite size.

Another objective of this project was to investigate the optimum ratio of organosilicate in P(VDF-TrFE)/ organosilicate composite fibrous membrane for the improvement of toughness of the membrane for wearable applications. From the study, it can be found that adding just a very small percentage (e.g. 2%) of organosilicate can significantly increase the mechanical toughness of the PVDF-TrFE membrane. However, adding more organosilicate does not further increase the mechanical toughness significantly.

In addition, it was found the speed of drum collector in electrospinning affect the tensile properties of P(VDF-TrFE) (without organosilicate) membranes. With faster drum collector's rotation speed, there is a tendency of increase in Young's modulus, tensile strength, and toughness in direction aligned with the principle fiber orientation. However, elongation at break in this direction decreased as collector speed increased. Opposite tendency was observed in the direction perpendicular to the fiber orientation (horizontal, H). Young's modulus, tensile strength, and toughness in horizontal direction decreased, elongation at break increased as the collector rotation speed increased. The tensile properties of P(VDF-TrFE)/Organosilicate composite membranes were however not so much affected by the rotation speed of drum collector.

The smart shoe prototype demonstrate the concept of using electrospun piezoelectric membrane for sensing foot pressure and body activity wirelessly. However, much further work is needed to achieve consistent measurements.

8. Recommendations for Future Studies

In the present study, the piezoelectric responses from the electrospun membranes are relat ively weak and inconsistent. This may be caused by the weak orientations of the dipoles in the piezoelectric membranes or the poor interfacial contacts between the the piezoelec tric membranes and the electrodes made of Aluminum foils. The Aluminum foils also m ake the sensor device unbreathable to moisture transmission. For further studies, it theref ore necessary to:

(1) Investigate how to apply additional polling during or after electrospinning to enhance the piezoelectricity;

(2) Develop breathable electrodes, which will have consistly good contacts with the piezo electric membrane.

Furthermore, it is necessary to further investigate the optimal percentage of organoslicate in P(VDF-TrFE) membrane. It was found that the addition of 2 wt% organosilicate resulted significant improvement in the mechanical toughness of the P(VDF-TrFE) membrane. Further increase of organosilicate percentage in the membrane did not result significantly higher mechanical toughness. Optimal percentage of organosilicate addition in terms of mechanical t oughness could be in between zero to two percent. In terms of piezoelectricity, it was found that the addition of 6 wt% organosilicate resulted the highest piezoelectric outputs among the samples with varying percentage of organosilicate from 2% to 10%, since greatest cr ystallite size was found when the addition was 6 wt% organosilicate. It appeared that pie zoelectric output is associated with the crystallite size. However, the mechanism of formi ng large size crystallite is not clear, which requires further investigation.

Lastly, further improvement of smart shoe prototype should made. The problem of charge drif ting should be solved. Furthermore, more sensors, instead of just one in the current set-u p, should be connected to map the foot pressure in different parts of the foot. Investigation of pressure input and signals output correlation should be carried out.

9. References

1. P. Stanley-Marbell, R. Marculescu, D. Marculescu, *IEEE. Trans. Comput*., **2003**, *52*, 966.
2. C. A. Winterhalter, J. Teverovsky, P. Wilson, J. Slade, W. Horowitz, E. Tierney, V. Sharma, *IEEE. Trans. Inf. Technol. B*, **2011**, *9*, 402.
3. Xiaoming Tao, Smart Fibres, Fabrics and Clothing, *Woodhead Fibre Series*, *Woodhead* **2001**.
4. Gopalsamy, C., Park, S., Rajamanickam, R., Jayaraman, S., *Virtual Reality*, **1999**, *4*, 152-168.
5. C. Linti, H. Horter, P. Osterreicher, H. Planck, *International Workshop on Wearable and Implantable Body Sensor Networks*, **2006**, 137.
6. M.Silva, A.Catarino, H.Carvalho, A.Rocha, J.Monteiro, G.Montagna, *Intelligent Textiles and Mass Customisation International Conference,* **2009**, 301-310.
7. Magenes, G., Curone, D., Caldani, L., Secco, E. L., *Annual International Conference of the IEEE-EMBC,* **2010**, 3594-3597.
8. D. Ryoo, Y. Kim, J. Lee, *Annual International Conference of the IEEE-EMBS*, **2005**, 2437-2440.
9. Kim, H., Kim, S. M., Son, H., Kim, H., Park, B., Ku, J., Sohn, J. I., Im, K., Jang, J. E., Park, J. J., Kim, O., Cha, S., and Park, Y. J., *Energy & Environmental Science*, **2012**, 8932-8936.
10. Sun, M., Fernstrom, J. D., Jia, W., Hackworth, S. A., Yao, N., Li, Y., Li, C., Fernstrom, M. H., and Sclabassi, R. J., *J Am Diet Assoc*, **2010**, *110*, 45-7.
11. Shenck, N. S., Paradiso, J. A., *Ieee Micro*, **2001**, *21*, 30-42.
12. Park, S., Jayaraman, S., *Ieee Engineering in Medicine and Biology Magazine*, **2003**, *22*, 41-48.
13. Lovinger, A. J., *Science*, **1983**, *220*, 1115-1121.
14. J. Kymissis, C. Kendall, J. Paradiso and N. Gershenfeld, *Second International Symposium on Wearable Computers*, **1998**, 132-139.
15. N. S. Shenck and J. A. Paradiso, *Ieee Micro*, **2001**, *21*, 30.
16. U. Stephen, *Measurement Science and Technology*, **1999**, *10*, R16
17. J. A. Paradiso, *Proceedings of the 43rd annual Design Automation Conference*, **2006**, 645-650.
18. Shenck, N. S., Paradiso, J. A., *Ieee Micro*, **2001**, *21*, 30-42.
19. Beeby, S. P., Tudor, M. J., and White, N. M., *Measurement Science and Technology*, **2006**, *17*, R175-R195.

20. A. Gefen, *Wounds*, **2007**, *19*, 350.

21. Fang, J., Niu, H. T., Lin, T., and Wang, X. G., *Chinese Science Bulletin*, **2008**, *53*, 2265-2286.

22. Choi, S. W., Kim, J. R., Ahn, Y. R., Jo, S. M., and Cairns, E. J., *Chemistry of Materials*, **2006**, *19*, 104-115.

23. Gopal, R., Kaur, S., Ma, Z. W., Chan, C., Ramakrishna, S., and Matsuura, T., *Journal of Membrane Science*, **2006**, *281*, 581-586.

24. X. Wang, J. Shi, Piezoelectric Nanomaterials for Biomedical Applications, *Springer Berlin Heidelberg*, **2012**, 135-172.

25. V. V. Kochervinskii, N. V. Kozlova, A. Y. Khnykov, M. A. Shcherbina, S. N. Sulyanov, K. A. Dembo, *Journal of Applied Polymer Science*, **2009**, *116*.

26. Fabrice, A., Schmitt, P. M., Gehin, C., Delhomme, G., McAdams, E., and Dittmar, A., *Transactions on Information Technology in Biomedicine IEEE*, **2005**, *9*, 325-336.

27. Chang, J., Dommer, M., Chang, C., and Lin, L., *Nano Energy*, **2012**, *1*, 356-371.

28. Staessen, J. A., Thijs, L., Fagard, R., O'Brien, E. T., Clement, D., de Leeuw, P. W., Mancia, G., Nachev, C., Palatini, P., Parati, G., Tuomilehto, J., Webster, J., and Systolic Hypertension Europe Trial Investigator, *Jama-Journal of the American Medical Association*, **1999**, *282*, 539-546.

29. Lawes, C. M. M., Vander Hoorn, S., Rodgers, A., and Hypertens, I. S., *Lancet*, **2008**, *371*, 1513-1518.

30. Li, D.; Xia, X. *AdV. Mater*. **2004**, *16*, 1151-1170.

31. Andrew, J. S., Clarke, D. R., *Langmuir*, **2008**, *24*, 670-672.

32. Andrew, J. S., Clarke, D. R., *Langmuir*, **2008**, *24*, 8435-8438.

33. C.R.Yang, Z.D. Jia, Z.C. Guan, L.M.Wang, *J. Power Sources*, **2009**, *189*, 716.

34. H.Na, Q.Y. Li, H. Sun, C.Zhao, X. Yuan, *Polym. Eng. Sci*., **2008**, *48*, 934.

35. H.Na, Q.Y. Li, H. Sun, C.Zhao, X. Yuan, *Polym. Eng. Sci*., **2009**, *49*, 1291.

36. F.A. He, M. Sarkar, S. Lau, J.T. Fan, H.L.W. Chan, *Polym. Test*.,**2011**, *30*, 436.

37. Yoon, S., Prabu, A. A., Ramasundaram, S., and Kim, K. J., Advances in Science and Technology, 2008, 60, 52-57. (2008). PVDF Nanoweb Touch Sensors Prepared Using Electro-Spinning Process for Smart Apparels Applications.

38. He, F. A., Sarkar, M., Lau, S., Fan, J. T., and Chan, L. H., *Polymer Testing*, **2011**, *30*, 436-441.

39. A. Baji, Y. W. Mai, Q. Li, Y. Liu, *Nanoscale*, **2011**, *3*, 3068-71.

40. D. Dhakras, V. Borkar, S. Ogale, J. Jog, *Nanoscale*, **2012**, *4*, 752-6.

41. V. V. Kochervinskii, *Polymer Science Series C*, **2008**, *50*, 93-121.

42. D. Edmondson, A. Cooper, S. Jana, D. Wood, M. Q. Zhang, *Journal of Materials Chemistry*, **2012**, *22*, 18646-18652.

43. Fang, J., Wang, X. G., and Lin, T., *Journal of Materials Chemistry*, **2011**, *21*, 11088-11091.

44. Rezakhaniha R., Agianniotis A., Schrauwen J., Griffa J., Sage D., Bouten C., Vosse F., Unser M. and Stergiopulos N., *Biomechanics and modeling in mechanobiology*, **2012**, *11*, 461-473. http://bigwww.epfl.ch/demo/orientation/

45. Y.B. Cai, Q. Li, Q.F. Wei, YB. Wu, L. Song, Y. Hu, *Journal of Materials Science*, **2008**, *43*, 6132-6 138.

46. J.H. Hong, E.H. Jeong, H.S. Lee, D.H. Baik, S.W. Seo, J.H. Youk, *Journal of Polymer Science Part B-Polymer Physics*, **2005**, *43*, 3171-3177.

47. Y.L. Liu, Y. Li, J.T. Xu, Z.Q. Fan, *ACS Applied Materials and Interfaces*, **2010**, *2*, 1759-1768.

48. D. Mandal, S. Yoon, K.J. Kim, *Macromolecular Rapid Communications*, **2011**, *4*, 831-837.

49. M. Lord, *J. Biomed. Engng*., **1981**, *3*, 91-99.

50. Y. Ahn, J.Y. Lim, S.M. Hong, J. Lee, J. Ha, H.J. Choi, Y. Seo, *Journal of Physics Chemistry C*, **2009**, *117*, 11791-11799.

51. J. I. Langford, A. J. C. Wilson, *J. Appl. Cryst.*, **1978**, *11*, 102-113.

52. R. Klein, J. Runt, Q. Zhang, *Macromolecules*, **2003**, *36*, 7220-7226.

53. V. Bharti, H. Xu, G. Shanthi, Q. Zhang, K. Liang, *J. Appl. Phys.*, **2000**, *87*, 452-461.

54. S. Guo, S. Lau, H. Chan, X. Zaho, C. Choy, *J. Appl. Phys.*, **2003**, *94*, 5566-5573.

55. X. Li, E. Kan, *Sensors and Actuators A: Physical*, **2010**, *163*, 457-463.